Republic of Iraq
Ministry of Higher Education and
Scientific Research
University of Babylon
College of Science
Department of Physics

Possibility of Employing Graphene Nano-Ribbons as a Sensor for Some Toxic Gases by DFT

A Thesis
Submitted to the Council of the College of Science, University of Babylon as a Partial Fulfillment of the Requirements for the Degree of Master in Science /Physics

By

Noor Al-Huda Saleh Hadi Jaber

B.Sc. Physics-University of Babylon

2017-2018

Supervised by

Prof. Dr.
Hayder Mohammed Abduljalil

Prof. Dr.
Rabab Saadoon Abdoon

2021 A.D *1443 A.H*

[قَالُوا سُبْحَانَكَ لَا عِلْمَ لَنَا إِلَّا مَا عَلَّمْتَنَا ۖ
إِنَّكَ أَنْتَ الْعَلِيمُ الْحَكِيمُ]

صدق الله العلي العظيم

سورة البقرة: الآية (٣٢)

Dedication

To

The great teacher and leader, our messenger Mohammed, and his family that God preferable and introduces among all human beings

To

My Father and Mother .... with great Love

To

My Brothers and Sisters .... with great Love

NOOR AL-HUDA

Acknowledgments

I should like to express my deep thanks to the Almighty God, ***ALLAH JALA JALALAH***, for what I have become.

I would like to express my deep gratitude and appreciation to my supervisor, ***Prof. Dr. Hayder Mohammed Abduljalil*** for suggesting the topic of the thesis, and continuing advice and guidance throughout this work. I would like to express my deep gratitude and appreciation to my supervisor**,** ***Prof. Dr. Rabab Saadoon Abdoon*** for continuing advice and guidance throughout this work.

I am grateful to *Mohammed Ayad* from environmental recharge and study center, Babylon, Iraq for his help.

I am grateful to lecturer *Mohammed Alsultani* of AL-Qasim Green University, Environmental Sciences College, for his help.

NOOR AL–HUDA

Summary

In present study, pure and doped graphene nano-ribbon were used to determined toxic gases which are bromine (Br_2), ammonia (NH_3) and carbon monoxide (CO). Present study investigates on a bity a use graphene nano-ribbon in pure and doped phase as a gas sensor and their use in renewable energy.

Quantum tools that used in the present study was Density Functional Theory (DFT) and Time Depending - Density Function Theory (TD-DFT). DFT using to compute ground state properties such as geometrical stricture, total energy, energy gap, ionization potential, electron affinity and adsorption energy. TD-DFT method was used to compute excitation state such as UV-Visible spectrum. Calculation of geometrical stricture show that all bond length of pure and doped nano-ribbon are in agreement with experimental result. Doped mechanism by sulfur (S) and aluminum (Al) atom make a modification properties of graphene structure nano-ribbon.

Theoretically, 116-atom nano-ribbon with a dimension of (N=4 and M=4) and the length of nano-ribbon equal (1.4 nm) was selected. The adsorption process was carried out for each of the following toxic gases (ammonia NH_3, bromine Br_2 and carbon monoxide CO). The nano-ribbons was doped with 4 sulfur atoms in specific locations for the purpose of improving sensitivity to the mentioned gases. Then the sulfur atoms were replaced by aluminum atoms for the same purpose.

Practically, the casting method was used to prepare thin films for each of the graphene G, aluminum Al and graphene-aluminum G-Al films with certain proportions of these mixtures. It was observed that graphene is stable for all wavelengths. It was also noted that the absorbance decreases with increasing in the proportion of aluminum. Al has the highest transmittance, opposite the graphene which has the lowest.

Adsorption energy calculation for pure graphene nano-ribbon shows that has high reactivity with Br_2 gas compared with CO and NH_3. Adsorption energy shows that Br_2 and CO has chemical interaction with surface of graphene nano-ribbon. NH_3 has physical interaction with surface of nano-system. Doped graphene nano-ribbons by S and Al modify sensitivity and this clear in S-doped. NH_3 interaction change from physical to chemical adsorption. Br_2 gas in all system has high reactivity with surface.

UV-visible calculations show that interaction gas molecule with surface of pure graphene nano-ribbon have a red shift. Al-doped nano-ribbon have a red shift of electromagnetic radiation. Finally, S-doped have blue shift of electromagnetic radiation.

Energy gap in the theoretical and experimental parts in our study has approximately equal values.

List of Contents

List of Tables

List of Figures

List of Symbols and Abbreviations

Symbol	*Description*
FET	Field-Effect Transistor
$\mathbf{V_{ext}}$	The External Potential
$\mathbf{\hat{H}^{core}}$	The Core Hamiltonian Operator
$\mathbf{\hat{H}_e}$	The Electronic Hamiltonian Operator
$\mathbf{\hat{T}_e}$	The Electronic Kinetic Energy Operator
$\mathbf{\hat{T}_n}$	The Nuclear Kinetic Energy Operator
$\mathbf{\hat{V}_{ee}}$	The Repulsive Electron– Electron Interactions Operator
$\mathbf{\hat{V}_{ne}}$	The Attractive Interactions Between Nuclei and Electrons Operator
$\mathbf{\hat{V}_{nn}}$	The Repulsive Nucleus- Nucleus Interactions Operator
$\mathbf{\nabla^2}$	The Laplacian Operator
$\mathbf{E_e}$	The Electronic Energy
$\mathbf{E_{nuc}}$	The Constant Nuclear Repulsion
$\mathbf{\hat{H}}$	The Hamiltonian Operator

$\mathbf{r_{AB}}$	The Distance Between Nuclei A and B
$\mathbf{r_{iA}}$	The Distance Between Nucleus A and Electron i
$\mathbf{r_{ij}}$	The Distance Between Electrons i and j
$\mathbf{V_{ext}(r)}$	External Potential
$\mathbf{Z_{A,B}}$	The Atomic Number of Atoms A and B
$\boldsymbol{\phi_s}$	A Linear Combination of Atomic Orbitals (Basis Functions)
$\boldsymbol{X^{GTO}}$	Gaussian Wave Function
$\boldsymbol{X^{STO}}$	Slater Wave Function
$\boldsymbol{m_A}$	The Mass of Atom A
$\boldsymbol{\psi_e}$	The Electronic Wave Function
2D	Two Dimensional
Abbreviations	
Al	Aluminum
S	Sulfur Atom
Br	Bromine Atom

NH_3	Ammonia Gas
Br_2	Bromine Gas
CO	Carbon Monoxide
CVD	Chemical Vapour Deposition
DFT	Density Functional Theory
$E_{(anion)}$	Energy of Anion Molecule
$E_{(cation)}$	Energy of Cation Molecule
E_0	The Ground-State Energy
EA	Electron Affinity
E_{ad}	Adsorption Energy
E_g	Energy Gap
E_{HOMO}	Energy of the Highest Occupied Molecular Orbital
E_{LUMO}	Energy of the Lowest Unoccupied Molecular Orbital
eV	Electron Volt
G 5.0	Gaussian 5.0

G	Graphene
GV5	Gauss view 5.0.8
$\hbar$	Dirack Constant
HF	Hartree-Fock
HOMO	Higher Occupied Molecular Orbital
HUMO	Higher Unoccupied Molecular Orbital
IP	Ionization Potential
Mo	Molybdenum Atom
Mol.	Molecule
N	Nitrogen atom
N	The Number of Electrons
STO	Slater Type Orbital
SWCNTs/MWCNTS	Single or Multi Walled Carbon Nanotubes
UV	Ultra-Violet
V (r, t)	Potential Energy

$\mathbf{v}(\vec{\mathbf{r}}_\mathbf{i})$	The External Potential for the Attraction of Electron
$\boldsymbol{\rho}(\mathbf{r})$	Electron Density
$\boldsymbol{\xi}$	The Orbital Exponent
$\boldsymbol{\psi}$	The Total Wave Function
$\boldsymbol{\psi}_\mathbf{i}$	Molecular Orbitals Wave Function

Chapter One

Introduction

Chapter Two

Theoretical Background

Chapter Three

Results and Discussion

Chapter Four

Conclusions and Future Works

References

Chapter One
Introduction

1-1 Introduction

Single-layer graphene contains of a carbon atom monolayer forming a 2D honeycomb - like structure. Every carbon atom in a monolayer graphene binds to three adjacent carbon atoms forming a 2D plane [1]. The edges of graphene can come in two forms: armchair or zigzag (see Figure 1.1). The monolayer graphene sheet is the smallest known material [2]. In-plane bonds with both carbon atoms are described as sp^2 hybridization. Since the carbon valence shell contains 4 electrons but it is only bonded to 3 nearest nearby carbon atoms (Figure 1.1b), the fourth bond of the carbon atoms bending and sharing electrons over the surface of the material. The supplemental unbound electrons form usually replaced π-orbitals [1].

These bound electrons form graphene's distinctive valence and conduction band structure (Figure 1.1a). The band structure and atomic structure of graphene are shown in Figure1.1a and Figure 1.1b, in both. Graphene's band structure is simulated using the nearby neighbor's tight binding model [3]. There are 6 points, known as Dirac points, where even the valence and conduction band of the graphene contact in the Brillouin zone. Therefore, the untrained monolayer graphene is a zero-band semiconductor gap [4]. However, band gaps can be presented into graphene by a variety of ways, including the incorporation of multiple stacked layers [5,6], strain [7,8] and very limited graphene layers decided to call graphene nano-ribbon [9].

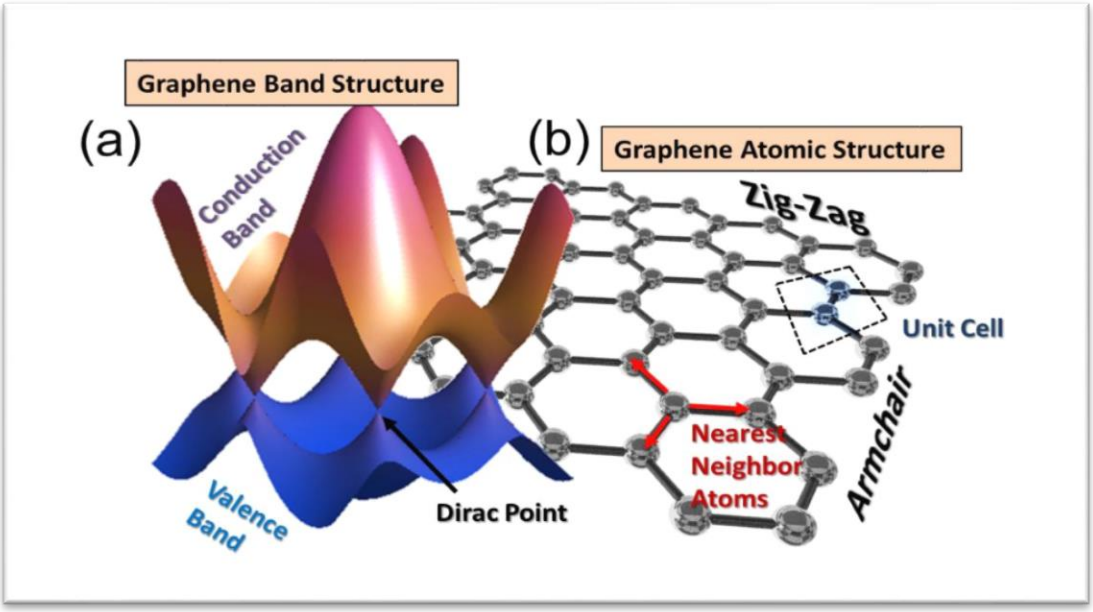

Figure (1.1): (a) Graphene band structure using a tight-binding model. (b) Graphene atomic structure [3].

1-2 Some of Graphene's Characteristics

The remainder outer-shell electron occupies a p_z orbital, which is parallel to the direction. These orbitals hybridize together form two half-filled bands of free-moving electrons, π and π^*, which are responsible for most of graphene's remarkable electronic properties [10]. Graphene sheets are positioned to form graphite with an energy gap of 0.335 nm [11].

Graphene sheets in solid form commonly show evidence of graphite (002) layering refraction. This is accurate for some single-walled nanostructures [12]. Even so, unlayered graphene with only (hk0) rings was found in the core of presolar graphite honey. Transmission Electron Microscopy (TEM) have shown facets of flaws in flat graphene sheets and suggest a role for two-dimensional [13].

The hexagonal lattice formation of an unconnected, single-layer graphene can be seen directly by the transmission electron microscopy (TEM) of graphene sheets suspended between metal grid bars [3]. Some of these pictures were shown a "rippling" of the flat sheet, with amplitude of about one nanometer. These ripples may also be inherent to the material due to instability of two-dimensional crystals [2,14,] or may originate from of the ubiquitous dirt seen in all graphene TEM images. Photoresist residues, that must be removed in order to obtain atomic-resolution images, may be the "adsorbates" observed in TEM images and it may explain the observed rippling.

The hexagonal structure is also seen in scanning tunneling microscope (STM) images of graphene supported on silicon dioxide substrates. The rippling seen in these images is caused by conformation of graphene to the subtrate's lattice, and is not intrinsic [15].

1-3 Potential Applications of Graphene

Because of its design and integration challenges, graphene remains a promising material for a wide range of potential applications, ranging from sensors to transistors [16,17]. Graphene even has a potential for energy harvesting and storage, which can be used as storage super capacitors [18] and also photodetectors as well as solar cells [19,20]. In addition, graphene has a number of other potential energy harvesting applications [21]. Although the applications are wide-ranging, the main focus of this work is on sensor applications.

1-4 Gas Sensor

Gas sensing has been a critical subject for a wide range of applications, like medical, industrial, military as well as aerospace applications. The presence of toxic and harmful gasses may lead to more serious accidents in both the industrial and household environments. There must have been some tool to effectively detect the

presence of these gases [22, 23]. The ultimate goal of gas detection is to achieve a high level of sensitivity with high resolution. The presence of a desired gas with very low concentrations should been detected. Furthermore, with solid-state gas sensors, such a high resolution of a gas sensor was not possible [24-26].

Nanomaterials are the promising candidates for the development of low operating temperature and low temperature gas sensors. The important parameter that defines the sensitivity of a gas sensing material is its surface-to-volume ratio, that is quite high for nanostructures. This high surface-to-volume ratio allows nanomaterials to effectively absorb detectable target molecules and make it suitable candidates and for development of efficient gas sensors [27]. In order to solve the problems identified in conventional solid-state gas sensors, graphene has emerged as such an exciting and promising candidate for more efficient detection of a wide range of organic and inorganic materials, including gases. Extraordinary electronic attributes of graphene and its derivatives make it an attractive candidate to substitute solid-state gas sensors [28-30].

1-5 Adsorption Process and its Varieties

Adsorption process considers one of the most important types of surface science, defined as a process when molecules and ions called adsorbate stick to the surface of the solid called adsorbent [31]. Adsorbate attached to the adsorbent surface, the degree of freedom and surface free energy reduced imbalance forces between two reactors [32]. The transfer of the adsorbate from of the liquid state to a solid state phase continues until the balance is reached between the amount of adsorbate bound in the adsorbent and the amount of adsorbate remaining in the solution. The degree of affinity between the adsorbent and the adsorbate decides this distribution with liquid and solid phases [33]. It is generally classified as a chemical and physical adsorption mechanism [34]. In chemical adsorption of a high amount with electron transport between two reaction

systems, high energy increases during this process ranged from 40-800 kJ/mol, so this process has been irreversible. All these results in the presence of a chemical bond between adsorbent and adsorbate [35]. There is weak van der Waals interactions in physical adsorption, no electron exchanges between them. A small amount of energy increases ranged from 5 to 40 kJ/mol. The absence of chemical bonding is an important factor in reducing energy. Physical adsorption was finally more acceptable to the multi-layer system [36].

1-6 Adsorption Process on 2-Dimention Nano-Materials

Since solid-state gas sensor has high sensitivity, wide range of application and low cost [37], the use of carbon nanotubes (CNTS) and semiconductor nanowire had also demonstrated a new generation of gas sensors in recent years [38]. CNTS is likely to be a large nanoscale sensor due to its fast response time and high room temperature sensitivity [39]. Similar to the good sensor properties of CNTS, graphene is considered to be an excellent sensor material due to its special properties, such as a two-dimensional structure that maximizes the interaction of layer adsorbates, low Johnson noise and the few crystal defects [40]. The graphene sample has also been reported to use as a gas sensor with the possibility of detecting carbon dioxide gas molecules, that have encouraged theoretical examination of a properties of graphene [41], and it has been shown that the donor or acceptor molecule on graphene can significantly change the electronic properties [42]. So when the molecules of gasses adsorbed on the graphene sheet, there are changes in resistance that makes it possible for graphene to be a solid state sensor for detection gas molecules. The ability of adsorption and the high surface-to-volume fraction of graphene makes it the ideal gas-sensing material. Recently, adsorption of different atmospheric gasses on graphene (like an active surface) had also recently been studied experimentally and theoretically [43]. A process of adsorption in pure graphene is really not that varied, and hence, regardless of any exception, using

pure graphene for adsorption mechanism of gas molecules may not be the best option. To conquer the insensitivity with these molecules to pure graphene, doped graphene, due to the formation of a three-dimensional structure, it is also established that the higher sensitivity of graphene to different molecules can be achieved by doping metals [44].

1-7 Graphene Nano-Ribbons Forms

Graphene nanoribbons (GNRs) are planar, finite, quasi-one-dimensional graphene structures. Figure (1.2) represents graphene family nanomaterials.

GNRs have been predicted to display high electrical and thermal conductivity, high breakdown current density, and low noise, which suggest that they can be used as an alternative to copper for integrated circuit interconnects. In general, GNRs show a bandgap that can be tuned by tailoring their width and edge structure. Zigzag GNRs are always metallic, while armchair GNRs can be either metallic or semiconducting [45]. In particular, the bandgap of armchair GNRs has been reported to scale with the inverse of the width. GNRs with zigzag edges are suggested to have localized states at the edges, which means that the electrical transport can be spin-polarized. This prediction combined with recent advances toward the scalable production of GNRs makes the introduction of graphene as a spintronic material feasible. GNRs have been produced chemically, in liquid phase by exfoliation, and by etching graphene using high-resolution electron beam lithography. The nanoribbons obtained by these methods are generally ∼10 nm wide and < 1 μm long in the case of liquid-phase produced ribbons. In most cases, the ribbons display an undefined or functionalized edge structure that affects the electronic properties [46].

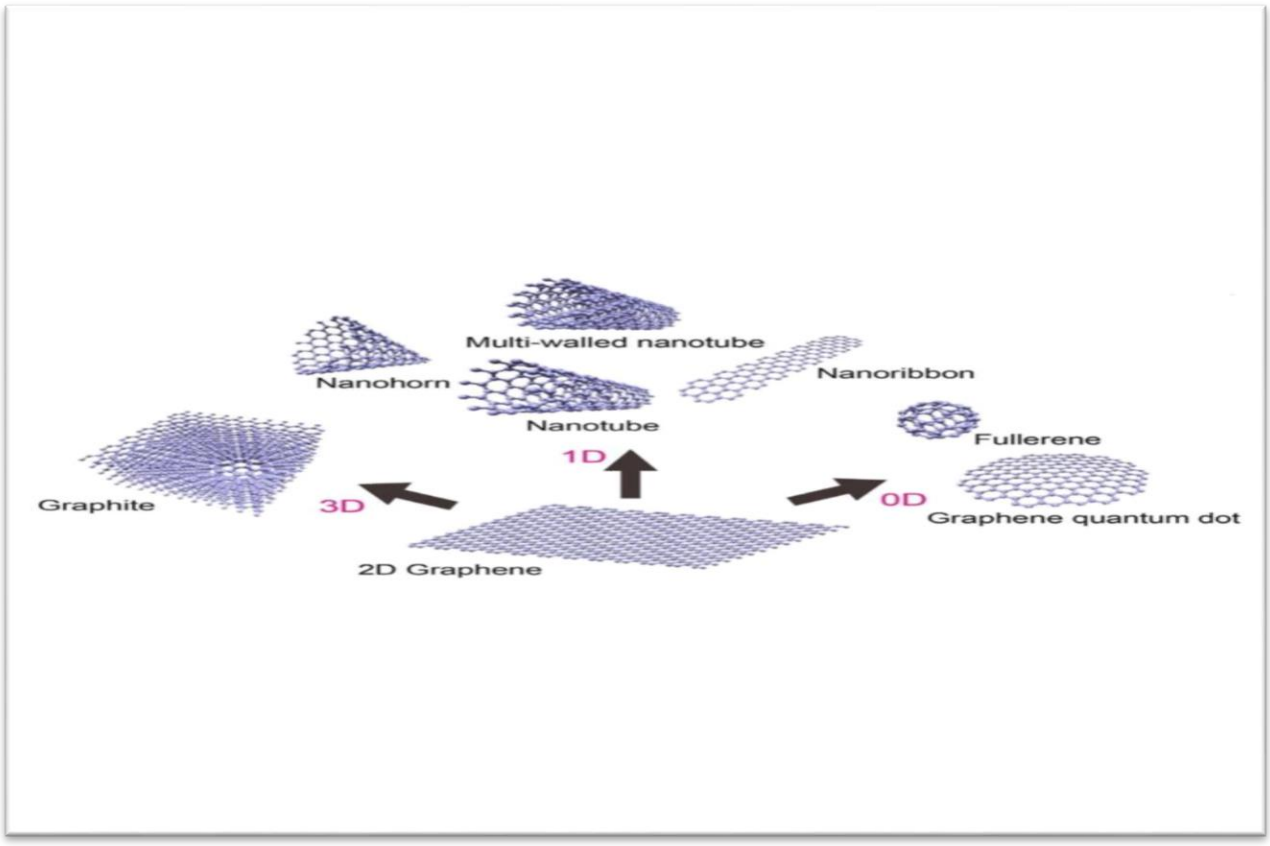

Figure (1.2): Graphene family nanomaterials structure[46].

1-8 Some Toxic Gases

In this work, the following toxic gases were investigated which are

1- ammonia (NH_3)
2- bromine (Br_2)
3- carbon monoxide (CO).

Below is a simplified explanation of each gas that was used:

1- Ammonia is lighter than air and has a characteristic pungent odor. Its chemical symbol is NH_3. Ammonia is highly soluble in water. Ammonia turns into a liquid at -33.35°C. The ammonia liquid boils at the same temperature, freezes and turns into a pure solid at -77.7°C. In its

transformation from liquid to gas again, it absorbs a large amount of heat from the external environment. Ammonia causes infections and irritations to the skin, eyes, nose, throat and upper part of the device respiratory. Figure (1.3 a) shows ammonia gas [47].

2- Carbon monoxide is a colorless, flavorless (tasteless), and odorless gas. It results from the partial oxidation process (incomplete combustion of carbon) and organic compounds such as coal, and this happens when oxygen is scarce, or when burning with a very high temperature. It is considered one of the highly toxic gases, and it is a form of carbon, as well as some oils and greases from machines and vehicles. It is a heterogeneous diatomic molecule because it contains two different elements, carbon and oxygen. This gas can also burn. It is worth noting that carbon monoxide and air (CO + air) mixtures are highly explosive. Figure (1.3b) shows carbon monoxide gas [48].

3- Bromine is a chemical element with symbol Br and atomic number 35, and it is located in the periodic table of the elements within the elements of the fourth period and in third place in the group of halogens. causes chemical burns to the skin, Inhalation of bromine gas also leads to irritation in the respiratory system, which leads to coughing, suffocation and shortness of breath; If inhaled in large quantities, it may cause death. Chronic exposure to bromine may cause acute bronchitis and worsen health [49]. Figure (1.3 c) shows Bromine gas.

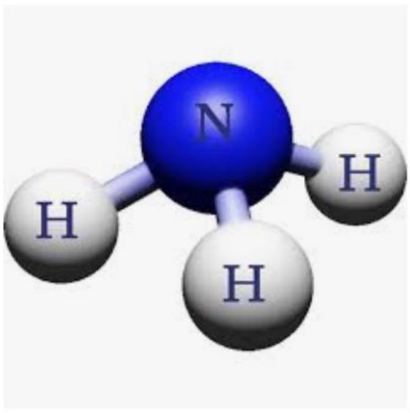

(a) NH_3

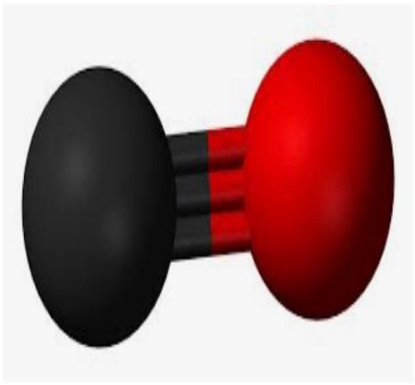

(b) CO

(c) Br_2

Figure (1.3): Represents the toxic gases used [47 – 49].

1-9 Previous Studies

- I. Khadije, et al. in (2012) studied examined the adsorption of CO, CO_2, NO and NH_3 particles on an armchair graphene nanoribbon (AGNR). The optimal adsorption sites and orientations of these molecules were determined on the AGNR. The adsorption and charge transfer energies and density of states (DOS) were obtained. NO, CO and CO_2 were absorbed the molecules acted as the acceptor, and the adsorbed NH_3 molecule acted as the donor [50].
- L. Xianqing, et al. in (2013) studied the adsorption behavior of H_2O, NH_3, CO and NO_2 on pristine graphene. The adsorption capacity (n) of particles on native graphene was calculated by statistical mechanics method. NO_2 contained the largest n of the order of 108 cm^2 among the four molecules on graphene at room temperature and a concentration of 1.0 ppm, but still about two orders of magnitude smaller than that of the graphene devices estimated from the experimental results. This is probably due to the strong binding of NO_2 to the edges of graphene with the termination of oxygen atoms with Eb with a size of 1.0 eV. Calculations of the

adsorption capacity of small polar molecules on native graphene and comparison with experimental values contributed to the understanding of the mechanism and design of graphene-based gas sensors [51].

- X. Huang, et al. in (2013) studied chemically reduced graphene oxide (CRG)-based NH_3 gas sensors. They used aniline to reduce graphene oxide (GO) to obtain CRGs attached with different states of polyaniline (PANI). The gas sensing properties of CRGs-based gas sensors were studied. The results indicate that the free CRG exhibited an excellent response to NH_3 and exhibited a high sensitivity to NH_3 with concentrations at the ppm level. CRG-based sensors showed a response of 37.1% upon exposure to 50 ppm of NH_3. Above all, CRG can be considered as an excellent sensor material for the detection of NH_3. In addition, the sensor can be easily fabricated by drip drying method, which holds great potential in various fields of gas sensing, due to its small size, low cost and portable characteristics [52].
- R. Ghosh, et al. in (2014) developed a highly sensitive, flexible and low cost ammonia sensor. The sensing element is based on chemically derived multilayer graphene and deposited on a 3-inch diameter filter paper. The sensor material was deposited on filter paper because it is a flexible substrate and also reduces cost. They obtained multilayer graphene by reducing graphene oxide (GO) with glucose. The synthetic sensor showed sensitivity to detect ammonia concentrations as low as 430 ppb. Sensor response characteristics as a function of ammonia concentrations (ranging from 400 to 4000 ppm) are reported in the paper. They also describe the variance in the response characteristics at the flat and curved positions of the sensors [53].
- C. Kuru, et al. in (2015) studied a large-scale graphene nano-ribbons (GNRs) network and applied it to gas sensing. A large area of nanoscale GNR network was produced to mask graphene made of silver nanowires (Ag NWs) and subsequent O_2 plasma etching. The GNR network shows significantly improved sensitivity to

ammonia compared to the original graphene layer. The gas detection sensitivity of the nanoscale GNR network is improved by decorating the GNR network with palladium (Pd) or platinum (Pt) nanoparticles, which exhibit a relative resistance response of 65% and 45%, respectively of ammonia (NH_3) in nitrogen (N_2) at room temperature as well as good reflectivity in air [54].

- C. N. Tien, et al. in (2016) studied the electronic properties and transport properties which were studied based on the density functional theory along with the non-equilibrium Greene function method. The absorption energy, density of states, electron density distortion, charge transfer, current and voltage properties, and transmission spectra were analyzed. CO and NH_3 molecules showed adsorption on GNRs with low adsorption energies and small charge transfer. The interactions between CO_2 and NH_3 molecules and GRNs are very weak. The results indicated that the sensitivity and selectivity of GRN-based gas sensors can be improved by modifying the electronic structures of graphene [55].
- S. Aghaei, et al. in (2017) studied the adsorption behaviors with toxic gas molecules (NO, CO, NO_2, and NH_3) on the graphene-like boron carbide (BC_3) investigated using first-principle density functional theory. The graphene-like BC_3 monolayer is a semiconductor with a band gap of 0.733 eV. The reserchers found that the amount of charge transfers on the adsorption of CO and NH_3 gas molecules on the BC_3 to be small. Each band gap changes in BC_3 due to CO and NH_3 interactions were only 4.63 % and 16.7 %, indicating that the BC_3 based sensor has such a low and moderate CO and NH_3 sensitivity, respectively [56].
- Z. Gao, et al. in (2018) studied a comprehensive theoretical study that was performed to investigate the adsorption properties of toxic gases (NO_2, NH_3, SO_3, and H_2S) by using single iron atom catalysts with three graphene-based supports. The adsorption geometry, adsorption energy, electronic and magnetic properties of the adsorption system are explored. In addition, the effects of support were

analyzed by d-band center and Fermi smoothness, and thermodynamic analysis which performed to consider the effect of temperature on gas adsorption. The support effects have a marked effect on the adsorption properties of the four types of toxic gases which are determined by the electronic structure of the graphene-based support, and the electronic structure can be characterized by the Fermi smoothness of the catalysts. The results could lay a basis for further study of the effects of graphene-based supports in single-atom catalysts for the development and design of new graphene-based supports using the idea of Fermi ductility [57].

- L. Fernanda, et al. in (2019) studied the adsorption mechanism of CO gas molecule with graphene dopant boron and nitrogen atoms. Their results indicate that the value of energy gap changed when gas molecule has interaction also band structure. CO gas molecule interaction physically with all graphene and dopant system [58].
- F. Subhan, et al. in (2019) investigated the possibility of selecting multiple toxic gases using a single substrate material. They explored the transport property of H_2, N_2, O_2, CO, CO_2, NO_2 and NH_3 gas molecules on two-dimensional (2D g-C_4N_3) graphitic carbon nitride. The homonuclear molecule such as H_2, N_2, and O_2 has a very weak adsorption energy, and carbon dioxide has an adsorption energy of 0.23 eV. In typical toxic gas particle adsorption systems, they find appreciable charge transfer. Moreover, by I-V curve calculations, they find a significant difference in current. The calculated current was 21, 13.11 and 16.16 μA for the CO, NO_2 and NH_3 systems with a bias voltage of 0.5 V. Their results indicated that 2D g-C_4N_3 could be a superior substrate material for sensing multiple toxic gases [59].
- N. T. Cuong in (2020) studied presented first-principle calculations made using a combination of DFT and NEGF methods to investigate the adsorption of CO_2 and NH3 molecules on the junctions of straight and U-shaped GNRs. It was found that the adsorption of CO and NH_3 on the straight GNRs at the edges of the dangling bond shows a chemical reaction behavior with high adsorption power. Besides, for

U-shaped ZGRNs without adsorption. Electrons in these positional states are nearly confined and do not contribute to conduction. However, for U-shaped GRNs with CO and NH_3 adsorbed on DB armchair edge defects, these states become undefined in the entire U-shaped junction. The current-voltage characteristics showed that the sensitivity and selectivity of the U-shaped GNRs gas sensors are significantly improved compared to the original GNR sensors [60].

- E. Salih, et al. in (2020) studied constricted zigzag graphene nano-ribbons (ZGNRs)-based sensor which constructed using the Atomic ToolKit Virtual NanoLab (ATK-VNL) and then used to detect nitrogen oxide (NO), nitrogen dioxide (NO_2) as well as ammonia (NH_3). They calculated the high absorption capacity for ZGNR-O-OH-NO_2 with −0.953 eV, when the highest transfer of charge has been found for ZGNR-OH-NO with −0.146 eV. Therefore, ZGNR-OH and ZGNR-O-OH can also be considered as promising NO and NO_2 gas sensors [61].
- A. I. Abdelamir, et al. in (2020) focused on the effect of two important factors using the three molecules weights (Mw) 4k, 8k and 20k (g mol-1) of polyethylene glycol (PEG) and reinforcement with a low load ratio of graphene oxide nanosheets (GONS) on the mechanical properties of a polymer matrix. A range of characterizations such as structural, rheological and mechanical properties were considered. These they were characterized using density and viscosity charges, Fourier transform infrared (FTIR), and X-ray diffraction (XRD), optical microscopy (OM) and ultrasound. FTIR results showed the most effective combination of PEGs and GONS, it also confirmed the significant strong relationship of PEGs with GONS. They were the crystal peaks of the pegs it was clearly presented in nanocomposites using XRD, while the GONS peak was not evident showing that of the whole complex. The despair of the GONS in the samples as presented. From the results they obtained nanocomposites samples lead

to a good medium for ultrasonic transmission especially in high molecules weights (20 carats), meaning that it provided good stability against mechanical and absorption waves [62].

- T. Y. Mi, et al. in (2020) studied the adsorption of toxic gas molecules: carbon monoxide (CO), carbon dioxide (CO_2) and ammonia (NH_3) on penta graphene nanoparticles (PGNRs) using first-principles methods. They studied the changes in the adsorption geometry, adsorption energies, charge transfer, electronic properties and electrical transport of PGNRs upon adsorption of these three gas molecules. The result showed that PGNRs are a good candidate for the detection of CO and NH_3 molecules when these two molecules are adsorbed in the region above the double bonds of PGNRs. Most interesting is that the PGNRs upon adsorption of CO and NH_3 molecules show a significant difference in transport coefficients near the Fermi level compared to that of pure PGNRs. These results open a new opportunity to develop a nanoscale gas sensor using pentagonal graphene nano-ribbons core materials. [63].
- V. Haridas, et al. in (2020) studied α -Fe_2O_3 functionalized Less defective graphene sheets were synthesized by cost-effective green solvent-assisted ultrasonic graphite-induced exfoliation followed by a hydrothermal method and its chemical ammonia gas sensing properties were investigated. A plausible sensing mechanism was suggested, signifying the role of both α-Fe_2O_3 and graphene leading to the synergistic response to NH_3 [64].
- F. Mofidia and A. Reisi-Vanani in (2020) studied electronic and structural proprieties for graphene oxide nano-ribbons. That were check out sensitivity of CO gas molecule towered graphene nano-ribbons. Their results indicated that CO gas molecule with GYO (graphene oxide) compared with pure GY (graphene) and GYO2 (graphene dioxide) also take place physical adsorption [65].
- J. Kim, et al. in (2021) studied the interaction of bromine of various types of

polycyclic aromatic hydrocarbons (PAHs) with oxygen atoms and graphene with oxygen atoms was estimated by calculating density functional theory and experimentally clarified by analyzing bromine of aromatic hydrocarbons using gas chromatography-mass spectrometry. In the experimental and theoretical bromination reaction of PAHs, the presence of the hydroxyl group increased the PAH reaction due to the electron-donating nature of the hydroxyl group. The effects of functional groups on reactivity were also confirmed in graphene. Their study for estimating the reactivity of bromination of graphene edges provided the basis for bromination of graphene edges [66].

- E. Salih and A. Ayesh in (2021) studied four armchair graphene nano-ribbons (AGNR) based sensor materials which have been manufactured using the Atomic ToolKit Virtual NanoLab (ATK-VNL) and then used to identify carbon monoxide (CO) and carbon dioxide (CO_2) gases. The results showed a significant increase in adsorption energy almost to 9 times non-doped systems for Pt–N-AGNR CO cases and also CO_2 for both Pt–H-AGNR and Pt–N-AGNR. As well as, they observed a rise of almost 13 times in adsorption energy for Pt–H-AGNR CO. In addition to the adsorption energy (E_{ads}), they examined the adsorption distance (D), the load transfer (ΔQ), the state density (DOS) and also the band structure to confirm the adsorption of CO and CO_2 on the four systems transfer (ΔQ), state density (DOS) as well as the band structure to verify the adsorption with CO and CO_2 on the four systems [67].
- R. Mehla, and S. Singh in (2021) studied the variability in the geometric and electronic properties of the graphene nano-ribbons (AGNRs) chair along with the pristine and phosphorous (P-AGNRs) configuration was determined in the presence of ammonia (NH_3). The calculations based on density functional theory were performed in order to detect and equalize the sensitivity of armchair-modified graphene nano-ribbons to NH_3 sensing. Furthermore, the variability in the geometric and electronic properties of AGNRs and P-AGNRs was analyzed by

considering the coherent energy, band structure, density of states, and conductivity. Their results showed that P-activated AGNRs can increase its sensitivity to NH_3 gas by an order of 106 times due to the improvement in conductivity [68].

- Y. Han, et al. in (2021) studied carbon dioxide and nitrogen oxide adsorption behaviors, and potential redox reactions on the surface of graphene pentahydrate by first principles calculations. The results showed that the carbon dioxide or nitrogen oxide molecule favors chemical adsorption on the surface of the graphene pentagram after overcoming the 0.046 eV or 0.037 eV energy barrier. The energy barrier for the complete reaction is expected to be only 0.375 eV under the Eley-Rideal mechanism and is well below 0.970 eV under the Langmuir-Hinshelwood mechanism, which is very close to the noble metal-catalyzed CO oxidation. Their results provided a new route not only to catalyze toxic molecules coexisting together but also to produce N_2O through the reaction of NO and CO on the PG surface, and will be useful for potential applications of PG-based catalyst in the future [69].
- S. J. Kheirabadi, et al., in (2021) used monolayer and bilayer armchair graphene nano-ribbons (AGNRs) (10 atoms wide) and studied their sensitivity in the presence of CO, O_2 and CO_2 gas molecules. With the Quantum espresso-5.3.0 package, architecture optimizations were done based on (DFT). Their results showed that the adsorption of CO, oxygen and CO gas molecules on the AGNR can be significantly modified in the bilayer AGNR with respect to the monolayer. These gas molecules showed a weak interaction with the AGNR atomic structure due to the large interaction distances. Thus, they concluded that graphene nano-ribbon (AGNRs) showed poor gas sensing in the presence of CO, O and CO_2 molecules. Meanwhile, bilayer AGNR showed different electronic properties compared to monolayer AGNR which makes it very sensitive and selective to the presence of O_2 and CO gases [70].

- M. A. Al-Seady, et al., in (2021) used density function theory calculations to calculate the ground state properties of a pure nano-doped aluminum (graphene/boron nitride) system. The hybrid function used in this study was (B3LYP) and the base group 6-31G*. Calculations of the bond length for the pure and doped nanosystem were in agreement with the experimental measurements. The adsorption energy calculations showed a low energy rise during the interaction between the gas molecule and the surface of the nanosystems. Also, their results showed that the adsorption type was physical. The molecular orbital energy is not affected during the reaction process. The charge transfer calculation also showed that the carbon dioxide molecule acts as a donor in the pure graphene system, boron nitride and graphene and acts as acceptor in boron nitride [71].

1-10 Aim of the Work

This study aims to design a theoretical sample of graphene and its derivatives for detecting some toxic gases as (NH_3, Br_2 and CO) in nature.

1-11 Steps to Achieve the Aim

Pure graphene nano-ribbon was design to determined sensitivity of toxic gases which are bromine (Br_2), ammonia (NH_3) and carbon monoxide (CO). Then nano-ribbon has been doped with four sulfur atoms in symmetric sites and was employed to detected the toxic gases. After that, sulfur atoms have been replaced with aluminum atoms for the same purpose.

1-12 Chapter's Overview

Chapter one illustrated an introduction to the graphene nano-ribbons and their properties, information about gas sensor, as well as adsorption and some previous studies in this field.

Chapter two is a theoretical background of the method used in present work with important equations. This chapter included the employed equations in calculating of the proposed structures with description for the used programs.

Chapter three the results and discussion, it included the description of designing of pure and doped graphene nano-ribbons and the final results of the structural, electronic and optical properties of the nano-ribbons under study.

Chapter four is the conclusions of the major findings in this study with some suggestions for the future research works.

Chapter Two
Theoretical Background

2-1 Introduction

Quantum mechanical methods can be divided into two categories: *ab* initio methods and semi empirical methods (SE). *Ab* initio methods include Hartree–Fock theory (HF), perturbation theory (PT), and density functional theory (DFT). These methods start with Schrodinger equation and carry out a complete integration, without introducing empirical factors derived from the experimental measurement [72]. While the semi-empirical methods have many omissions in addition to the introduction of some experimental factors in the calculations. For the past 30 years DFT has been the dominant method for the quantum mechanical simulation of periodic systems. In recent years it has also been adopted by quantum chemists and is now very widely used to simulate of the energy surfaces in molecules.

Throughout the theoretical chemistry and physics, the fundamental law of physics is combined with mathematical methods for studying the progression of chemical relevance and physical [73]. Molecular modeling methods and physicians are still widely used to computationally investigate many properties like molecular energy, molecular geometry, electronic structure, electron and charge distribution, ultraviolet (UV) and the physical properties of biological, inorganic, organometallic, polymeric, catalytic and also other molecular systems [74].

2-2 The Schrödinger Equation

The Schrödinger equation which was proposed by Erwin Schrödinger in 1925 is central to the evolution of quantum mechanics theory. Any problem with the electronic structure of the matter is [75]:

$$\widehat{H}\,\Psi = \mathrm{E}\,\Psi \qquad (2-1)$$

where Ψ is a wave function, it expresses the mathematical structure of de Broglie wave associated also with particle, $\hat{H}$ is the Hamiltonian operator, and E is the total energy of the system. Once the Schrödinger equation is solved, all electronic properties of the system can be calculated. The Hamiltonian operator, H, consists of two terms the kinetic energy of the electrons and the nuclei (T) and the potential energy components (V) [75].

$$\hat{H} = \hat{T} + \hat{V} \qquad (2-2)$$

$$\hat{H} = \hat{T}_e + \hat{T}_n + \hat{V}_{ne} + \hat{V}_{ee} + \hat{V}_{nn} \qquad (2-3)$$

where ($\hat{T}_e$) and ($\hat{T}_n$) are the kinetic energy operators of the electrons and nuclei, respectively. ($\hat{V}_{ne}$) the Coulomb attraction between the nuclei and electrons, ($\hat{V}_{ee}$) the Coulomb repulsion between electrons, ($\hat{V}_{nn}$) the Coulomb repulsion between nuclei.

The kinetic energy operators are represented as [75]:

$$\hat{T}_e = -\frac{\hbar^2}{2m_e}\sum_i \nabla_i^2 \qquad (2-4)$$

$$\hat{T}_n = -\frac{\hbar^2}{2M_A}\sum_A \nabla_A^2 \qquad (2-5)$$

where: m_e and M_A are the electron and nuclear masses, respectively, ∇_i^2 is the Laplacian operator of i electrons, which in Cartesian coordinates has the form [75]:

$$\nabla_i^2 = \frac{\partial^2}{\partial x_i^2} + \frac{\partial^2}{\partial y_i^2} + \frac{\partial^2}{\partial z_i^2} \qquad (2-6)$$

The potential energy operators are represented as [75]:

$$\hat{V}_{ne} = -\sum_A \sum_i Z_A \frac{e^2}{r_{Ai}} \qquad (2-7)$$

$$\hat{V}_{ee} = \sum_{i<j} \frac{e^2}{r_{ij}} \qquad (2-8)$$

$$\hat{V}_{nn} = \sum_{A<B} Z_A Z_B \frac{e^2}{R_{AB}} \qquad (2-9)$$

where $r_{ij} = |\vec{r_i} - \vec{r_j}|$ and Z_A is the charge of nuclei A, r_{Ai} is the distance between nucleus and electron, r_{ij} is the distance between i electron and j electron and R_{AB} is the distance between A and B nucleus.

The first major step in simplifying the general molecular problem in quantum mechanics is the Born-Oppenheimer approximation. This approximation is based on the fact that the nuclear masses are much greater than those of the electrons. Therefore, nuclei move much more slowly and they are nearly fixed compared with the electrons motion [76].

2-3 Hartree - Fock (HF) Methods

It is necessary to calculate the many-electron wave functions for the system using the time-independent Schrödinger equation to describe the quantum mechanical behavior of all electrons in the systems [77]. To solve the Schrödinger equation for all electrons in a system requires solving many of simultaneous differential equations [78]. Since this calculation is very difficult so it needs simplifying the methods and the problem itself. In 1928 Hartree made such a simplification through an iterative self-consistent field (SCF) method by making an assumption about the form of the many-electron wave functions. In a uniform system the wave functions would take the form of simple plane waves. According to the variation principle, if a given system is described by a set of unknown parameters, the set of parameter values which correctly describe the ground state of the system

is just that set of values which minimize the total energy, this can be expressed as [77-80]

$$E_{\Phi} = \frac{\langle \Phi | \hat{H} | \Phi \rangle}{\langle \Phi | \Phi \rangle} \geq E_o \qquad (2-10)$$

where E_Φ is the lowest-energy eigen value of the eigen function Φ and E_o is the ground-state energy. Using this theorem, the exact ground-state wave function is approximated from the eigen function that gives the lowest energy. Hartree found the Hamiltonian equation of the many-electron system and it was possible to treat each electron separately as a single-particle.

The wave function of Hartree-Fock approach can be written in a compact way as a Slater determinant. The determinant considers the spin of all the electrons and the Pauli exclusion principle. Equation (2 - 11) is an example of a Slater determinant for a system of N-electrons [79,80]:

$$\Psi = \frac{1}{\sqrt{N!}} \begin{vmatrix} \Psi_1(1)\alpha(1) & \Psi_1(1)\beta(1) & \Psi_2(1)\alpha(1) & \Psi_2(1)\beta(1) & \dots\dots & \Psi N(1)\alpha(1) & \Psi_N(1)\beta(1) \\ \Psi_1(2)\alpha(2) & \Psi_1(2)\beta(2) & \Psi_2(2)\alpha(2) & \Psi_2(2)\beta(2) & \dots\dots & \Psi_N(2)\alpha(2) & \Psi N(2)\beta(2) \\ . & & . & & & . & \\ . & & . & & & . & \\ \Psi_1(N)\alpha(N) & \Psi_1(N)\beta(N) & \Psi_2(N)\alpha(N) & \Psi_2(N)\beta(N) & \dots\dots & \Psi_N(N)\alpha(N) & \Psi_N(N)\beta(N) \end{vmatrix} \qquad (2 - 11)$$

where Ψ is the electronic wave function, α and β are the spin up and spin down of electrons, respectively, and $\frac{1}{\sqrt{N!}}$ is a normalization factor.

The next step in Hartree-Fock method is introducing the molecular orbital expansion and determining the corresponding coefficients based on the variation

theorem [81]. Solving the Hartree-Fock equation using the iterative process of the self-consistent-field (SCF) producer yields the molecular orbitals ψ (r_i) [79,80].

$$F\Psi_i(\vec{r}) = \varepsilon_i\Psi_i(\vec{r}) \qquad (2-12)$$

For closed shell systems the Fock operator F takes the form:

$$F = h + \sum_{l=1}^{n/2}(2J_l - K_l) \qquad (2-13)$$

The Coulomb operator J_l and the exchange operator K_l are defined as [79,80]:

$$J_l\Psi(\vec{r}) = \int \frac{\Psi_l^*(\vec{r})\Psi_l(\vec{r'})}{\left|\vec{r}-\vec{r'}\right|} dV'\Psi(\vec{r}) \qquad (2-14)$$

$$K_l\Psi(\vec{r}) = \int \frac{\Psi_l^*(\vec{r})\Psi_i(\vec{r'})}{\left|\vec{r}-\vec{r'}\right|} dV'\Psi(\vec{r}) \qquad (2-15)$$

A further restriction involves expanding the molecular orbitals in terms of basis functions φ_i , linear combinations of one-electron functions according to the linear combination atomic orbital (LCAO) method. Thus an individual molecular orbital is defined as [79,80]

$$\Psi_i = \sum_{\mu=1}^{N} C_{\mu i}\phi_\mu \qquad (2-16)$$

where $C_{\mu i}$ represents the molecular orbital expansion coefficients. The basis functions φ_i are also chosen to be normalized.

For orbital expansion an appropriate set of basis functions have to be selected, with that the coefficients $C_{\mu i}$ may then be adjusted to minimize the total electronic

energy calculated from the many-electron wave function. The resulting value of the energy will then be as close as possible to the exact energy E_o of the ground state of the system within the selected limitations [82].

$$E(\Phi_1, \Phi_2, \dots\dots, \Phi_N) \geq E_o \qquad (2-17)$$

The equality sign is applied only in case Ψ_i is the exact ground state function.

2-4 Density Functional Theory (DFT)

The density functional theory (DFT) is presently the most successful approach to compute the electronic structure of matter. Applicability ranges from atoms, molecules and solids to nuclei and quantum and classical. In its original formulation, the density functional theory provides the ground state properties of a system, and the electron density plays a key role. DFT predicts a great variety of molecular properties, molecular structures, vibrational frequencies, atomization energies, ionization energies, electric, magnetic properties and reaction paths, etc. [83].

In 1927, the functional predecessor to density theory was the Thomas-Fermi model, developed by Thomas and Fermi. Thomas and Fermi are calculated the energy of an atom by representing its kinetic energy as a function of the electron density, combining this with the classical expressions for the nuclear-electron and electron-electron interactions, which can both also be represented in terms of the electron density [84, 85].

DFT derives properties of a many particle system as a functional of electron density$\rho(r)$. Electron density is the number of electrons per unit volume for a given state. It is dependent only on three coordinates regardless of the number of electrons of the system, as [85]:

$$N = \int \rho(\vec{r}) d\vec{r} \qquad (2-18)$$

The fundamental concepts of DFT rely on the ground state energy and all other ground state electronic properties are uniquely determined by the electron density. Furthermore, the exact ground state of the system corresponds to the electronic density for minimal total energy.

2-4-1 Hohenberg-Kohn Theory

Hohenberg-Kohn results reduced the problem of solving the many body Schrödinger equations to the problem of minimizing a density functional. They proved that in 1964 a many-electron system of the ground state can be determined by the ground state electron density ρ(r) [84,86,87].

Theorem I: The ground state energy of a many-electron system is a unique functional of ground state electron density ρ(r).

Theorem II: The functional of ground state energy is minimized by the ground state electron density ρ(r) for a many-electron system.

Any ground state properties (according to these theorems) of a many electron systems can be expressed in terms of the ground state electron density ρ(r). The ground state energy functional E_V can be described as [88,89]:

$$E_V[\rho] = \int \rho(\vec{r})\, V_{ext}(\vec{r}) d\vec{r} + F_{HK}[\rho] \qquad (2-19)$$

where $F_{HK}[\rho]$ is a functional of ρ(r) to be determined which includes kinetic energy and all the electron-electron interactions. Considering of the particle conservation, the variation of ground state energy satisfies the following principle [88,89]:

$$\delta\left\{E_V[\rho] - \kappa\left[\int \rho(\vec{r})d\vec{r} - N\right]\right\} = 0 \qquad (2-20)$$

which give.

$$\kappa = \frac{\delta E_V[\rho]}{\delta\rho(\vec{r})} = V_{ext}(\vec{r}) + \frac{\delta F_{HK}[\rho]}{\delta\rho(\vec{r})} \qquad (2\text{ - }21)$$

where (κ) is the chemical potential. Note that $F_{HK}[\rho]$, where F_{HK} is a universal functional of the electron density. The ground state electro properties of many-electron system can be obtained exactly from Eq. (2 - 20) and Eq. (2 - 21).

Hohenberg-Kohn theorem assumes that F_{HK} exists, but the actual form of F_{HK} is unknown and must be approximated.

2-4-2 Kohn-Sham Equations

The energy functional $F_{HK[\rho]}$ (according to Hohenberg and Kohn) of an interacting many-electron system can be expressed as [90,91]:

$$F_{HK}[\rho] = T[\rho] + \frac{1}{2}\iint \frac{\rho(\vec{r})\rho\left(\overrightarrow{r'}\right)}{\left|\vec{r} - \overrightarrow{r'}\right|} d\vec{r}d\overrightarrow{r'} + E_{xc}[\rho] \qquad (2-22)$$

where T[ρ] is the kinetic energy of the system; the second term is the classical Coulomb energy، the third term $E_{xc[\rho]}$ is the exchange-correlation energy which describes the non-classical interaction of electrons including all the many-body effects.

Now, $\rho(\vec{r})$ can be expressed for a non-interacting system by a set of auxiliary orthogonal function $\psi_i(\vec{r})$ as [90,91]:

$$\rho(\vec{r}) = \sum_i \psi_i^*(\vec{r})\psi_i(\vec{r}) \qquad (2-23)$$

and $\langle\psi^i|\psi^j\rangle$=$\delta_{ij}$.

The Kohn-Sham kinetic energy was given by [89]:

$$T_{KS}[\rho] = -\frac{\hbar^2}{2m}\int \sum_{i=1}^{N} \psi_i^*(\vec{r})\nabla^2\psi_i(\vec{r})d\vec{r} \qquad (2-24)$$

Considering the many-body interaction, the true kinetic energy T[ρ] in equation (2–22) is not equal to T_{KS}[ρ]. The difference between them can be combined with exchange-correlation functional E_{xc}[ρ] as [89-92]:

$$E_{XC}[\rho] = E_{xc}[\rho] + T[\rho] - T_{KS}[\rho] \qquad (2-25)$$

and the ground state energy functional can be written as [92]:

$$E_V[\rho] = T_{KS}[\rho] + \frac{1}{2}\iint \frac{\rho(\vec{r})\rho(\overrightarrow{r'})}{|\vec{r}-\overrightarrow{r'}|}d\vec{r}d\overrightarrow{r'} + E_{XC}[\rho] + \int d\vec{r}\,\rho(\vec{r})V_{ext}(\vec{r}) \qquad (2-26)$$

By applying the variation principle to equation (2–26):

$$\frac{\delta}{\delta\psi_i^*(\vec{r})}\left\{E[\rho] - \int d\vec{r}\sum_i \varepsilon_i\psi_i^*(\vec{r})\psi_i(\vec{r})\right\} = 0 \qquad (2-27)$$

This leads to the Kohn-Sham equations:

$$\left\{-\frac{\hbar^2}{2m}\nabla^2 + \int \frac{\rho\left(\overrightarrow{r'}\right)}{\left|\vec{r}-\overrightarrow{r'}\right|}d\overrightarrow{r'} + V_{XC}[\rho] + V_{ext}(\vec{r})\right\}\psi_i(\vec{r}) = \varepsilon_i\psi_i(\vec{r}) \qquad (2-28)$$

where $V_{XC}[\rho]$ is the exchange-correlation potential which has been modified to include all the difference between the interacting and non-interacting kinetic energy in equation (2 – 28), $V_{XC}[\rho]$ takes the form [92] :

$$V_{XC}[\rho] = \frac{\delta E_{XC}[\rho]}{\delta \rho(\vec{r})} \qquad (2-29)$$

It should be noted that, the Kohn-Sham equation has to be calculated self-consistently considering that the wave function $\psi_i(r)$is influenced by the electron density $\rho(r)$ included in Hamiltonian. Through solving a set of Kohn-Sham equations (2 – 28) self-consistently, one can obtain the total energy of the system [92]:

$$E = \sum_{i}^{N} f_i \varepsilon_i - \frac{1}{2} \iint \frac{\rho(\vec{r})\rho(\overrightarrow{r'})}{|\vec{r} - \overrightarrow{r'}|} d\vec{r} d\overrightarrow{r'} + E_{XC}[\rho] - \int d\vec{r}\, \rho(\vec{r}) V_{ext}(\vec{r}) \qquad (2-30)$$

The physics of Kohn-Sham equation is unlike that of Schrödinger equation. The significance of Kohn-Sham equations consists that, it reduced an interacting many-body problem to a set of independent equations which describes the state of single electron in the effective potential of other electrons.

The major problem of DFT is to find the exchange-correlation energy (E_{XC}), used so far as a mathematical term. This term includes all the effects of exchange and correlation interactions, such as Pauli exclusion between electrons with same spin orientations, and the instantaneous reaction of electrons with opposite spins. If the exact exchange-correlation function is known, the system is solved exactly. As previously noted, this function is from the difference of the Hamiltonian between the interacting many-electron systems and the non-interacting single electron system [85].

2-4-3 Local Density Approximation

The local density approximation (LDA) [85,93] is the simplest approximation to $E_{XC}[\rho(r)]$, which assumes that the system is a homogeneous electron gas and E_{XC}

[ρ(r)] depends only on the local value of electron density. Therefore, E_{XC} [ρ(r)] can be written in a simple form [88]:

$$E_{XC}^{LDA}[\rho] = \int \rho(\vec{r})\, \varepsilon_{XC}\big(\rho(\vec{r})\big) d\vec{r} \qquad (2-31)$$

2-4-4 Local Spin Density Approximation (LSDA)

The local spin density approximation (LSDA) defines the exchange correlation potential in terms of the density of α and β spins and was developed for calculating the properties of open-shell systems [90]:

$$E_{XC}^{LSDA}\big[\rho_\alpha, \rho_\beta\big] = \int \rho(\vec{r}) \varepsilon_{XC}\big(\rho(\vec{r})_\alpha, \rho(\vec{r})_\beta\big) d\vec{r} \qquad (2\text{ - }32)$$

where ε_{XC} is the exchange-correlation energy per particle. LSD approximation provides better results than HF for certain properties such as equilibrium structures, vibrational frequencies and dipole moment.

In general, the LSDA provides reliable information for those systems that closely resemble a uniform electron gas, namely those in which the density varies slowly with position. However, in reality, atomic and molecular systems do not possess uniform electron densities and thus more sophisticated models are required.

2-4-5 The General Gradient Approximation

Generalized gradient approximations (GGA's) for the exchange-correlation energy improve upon the local spin density (LSD) description of atoms, molecules, and solids. present a simple derivation of a simple GGA, in which all parameters (other than those) in LSD are fundamental constants [90].

$$E_{XC}^{GGA}\big[\rho_\alpha, \rho_\beta\big] = \int f\big(\rho_\alpha, \rho_\beta, \nabla\rho_\alpha, \nabla\rho_\beta\big) d\vec{r} \qquad (2-33)$$

This functional generally offer an improvement over the LSDA since they account for the variation of density with position. To simplify the problem, (E_{XC}) is often written as the sum of an exchange (E_X) and correlation (E_C) terms [88]:

$$E_{XC} = E_X + E_C \qquad (2-34)$$

The exchange-energy functional can then be obtained from the HF exchange term with the Kohn-Sham orbitals instead of the HF orbitals and approximate solutions for (E_C) are sought. Various exchange and correlation functionals have been developed independently and can be combined in various ways. For instance, one popular (GGA) functional is BLYP, where Becke's (in 1988) exchange functional [93] is paired with the Lee-Yang-Parr correlation functional.

2-4-6 The Hybrid Functional

The hybrids functional are very successful in describing a wide range of molecular properties accurately. In large molecules and solids, however, calculating the exact (Hartree-Fock) exchange is computationally expensive, especially for systems with metallic characteristics.

The most popular hybrid functional, B3LYP, [88,90-92,94], uses Becke's 1988 exchange functional (E_X^{B88}) and Lee, Yang and Parr's correlation functional (E_C^{LYP}) as gradient corrections to the LSDA exchange and correlation functional [95].

$$E_{XC}^{B3LYP} = (1-a)E_X^{LSDA} + aE_{XC}^{\lambda=0} + bE_X^{B88} + cE_C^{LYP} + (1-c)E_C^{LSDA} \quad (2-35)$$

where the three parameters, a=0.20, b=0.72 and c=0.81.

Here a: specified the amount of exact exchange.

b and c control the contribution of exchange and correlation, respectively.

2-5 The Wave Function

The wave function Ψ is not physically observable, but its square $[\Psi]^2$ can be interpreted as the probability density, which yields a probability when multiplied by the volume of a region. Acceptable wave function for a system has to be orthogonal to each other and normalized (orthonormal) [96]:

$$\int \Psi_i \Psi_j dx_N = \langle \Psi_i | \Psi_j \rangle = \delta_{ij} \qquad (2-36)$$

The energy of a wave function can be calculated as an expectation value of the Hamiltonian operator [96]:

$$E = < \hat{H} > = \frac{\int \Psi^* \hat{H} \Psi \, dt}{\int \Psi^* \Psi \, dt} \qquad (2-37)$$

The wave function Ψ describes a many particle systems.

2-6 Basis Set

Most methods require a basis set be specified. The exceptions consist of a few methods for which the basis set is defined as an integral part of the method, most semi empirical methods use a predefined basis set. When ab initio or density functional theory calculations are done, a basis set must be specified, a basis set is a set of functions used to describe the shape of the orbitals in an atom. Molecular orbitals and entire wave functions are created by taking linear combinations of basis functions and angular functions. The type of calculation performed and basis set chosen are the two main factors in determining the accuracy of the results [97,98].

2-6-1 Slater Type Orbitals (STO's)

The Slater type orbitals have the form [99,100]:

$$\chi^{STO} = N r^{n-1} e^{-\xi r} Y_{lm}(\theta, \varphi) \qquad (2-38)$$

Here n, is a principal quantum number and ξ is a constant related to the effective charge of the nucleus. Y_{lm} is a spherical harmonic which describes the angular part of the wave function. Slater type functions show a correct behavior nears the nuclei at r → 0 with a discontinuous behavior.

2-6-2 Gaussian Type Orbitals (GTO's)

Gaussian type orbitals (GTOs) can be written in terms of Cartesian coordinates as [98-100]:

$$\chi^{GTO} = Nx^{lx}y^{ly}z^{lz}e^{-\xi r^2} \qquad (2-39)$$

where: N is a normalization factor, the sum of lx, ly and lz determines the type of orbitals. ξ represents the orbital exponent that show compact large ξ or diffuse small ξ is the resulting function, r^2 dependence in the exponential is a deficiency of the GTO's with respect to the Slater-type orbitals STO's [101,102].

Subsequently, the tail of the wave function in the GTO is represented poorly. A rough estimate says that three times as many GTO's as STO's are requird in order to reach the same level of accuracy. One of the disadvantages of STO's is that many-center integrals such as Coulomb and HF-exchange terms are difficult to compute with STO's. Subsequently it does not play a role in modern wave function based quantum chemistry codes. One of the advantages of the Gaussian basis set is that the product of two Gaussian functions is another Gaussian function. As a result, for the calculations of Coulomb and HF-exchange terms the analytical solution is available for the Gaussian functions. Therefore, the GTO basis function in HF and related methods is popular because very efficient algorithms exist for analytically calculating the many-center integrals. In order to improve the GTO basis sets, one

usually employs a contracted GTO basis set, in which several primitive Gaussian functions are mixed to gives a contracted Gaussian function (CGF) as [103]:

$$\chi_j^{CGF} = \sum_i^M C_{ij}\chi_a^{GTO} \qquad (2-40)$$

Here, M is the number of Gaussian primitives used in a linear combination. The basis sets used in Gaussian are classified into: minimal basis sets, split valence sets, Polarization and Diffuse Functions and others [103].

2-6-2.1 Minimal Basis Sets

The minimal basis sets represent all orbitals up to and including valance orbitals, it is the minimum number of basis functions χ needed to describe the ground states of the component atoms in a molecule for example (1s, 2s and 2p on carbon atom). The STO-3G is a common minimal basis set. In these basis sets, the same number of Gaussian primitives comprises core and valence orbitals [104,105].

2-6-2.2 Split-Valence Basis Sets

A split-valence basis sets of the inner-shell atomic orbitals are represented by one basis function and the valence orbitals are represented by two or more basis functions (Pople basis sets) [93,100]. One easy method to extend a basis set is to increase the number of basis functions used per orbital. Split-valence basis sets employ more than one basis function of variable orbital exponents for each valence orbital and only one basis function for each core orbital. For instance, the valence double-zeta (VDZ) basis set uses two basis functions per valence orbital while the valence triple-zeta (VTZ) uses three, and so on. Another example of the k-lmnG basis sets developed by Pople and co-workers, here, k represents the number of primitive Gaussians used for each core orbital while l, m and n represent the primitives used for the valence orbitals. For instance, the 6-31G basis set uses a set

of 6 primitives contracted to one basis function for each core orbital and a split-valence of 3 and 1 primitives for the valence orbitals. While the split valence basis sets provide a better description of the molecular orbitals because they for variable atom size, they are still not able to provide a balanced basis set of their own [103].

2-7 Structure Properties

The highest occupied molecular orbital (HOMO) is the molecular orbital of highest energy that is occupied by electrons. The lowest unoccupied molecular orbital (LUMO) is the molecular orbital of lowest energy that is not occupied by electrons. The HOMO and LUMO are important in determining such properties as molecular reactivity and the ability of a molecule to absorb light [104].

2-7-1 Geometrical structures

All molecules possess geometry, characterized by [104-106]:

1. Number and types of atoms
2. Number and types of bonds
3. Relevant bond lengths r: $0 \leq r \leq \infty$ (in units of Angstroms)
4. Relevant bond angles θ: $0 \leq \boldsymbol{\theta} \leq 180^{\circ}$ (in units of degrees)
5. Relevant dihedral angles: $-180^{\circ} \leq \boldsymbol{\phi} \leq 180^{\circ}$ (an angle between four atoms, which signifies the 3-dimensional shape of the molecule).

Geometry optimization is a standard chemistry-physical calculation to find the lowest energy or largest relaxed conformation for a molecule. The approach is involving an iterative process, at each step, the molecular geometry is modified slightly and the energy of the molecule is compared with the last cycle. The computer moves the molecule a little, calculates the energy, moves it a little more, and keeps

going until it finds the lowest energy. This is the minimum energy of the molecule and obtained at the optimized geometry [107,108].

2-7-2 Total Energy (E_{tot})

The total energy for a system is the sum of total kinetic and potential energies, at the optimized structure that the total energy of the molecule must be at the lowest value because the molecule is at the equilibrium point. This means that the resultant of the effective forces is zero [109,110]

2-7-3 Energy Gap (E_{gap})

Energy gap is defined as the difference of energy between the bottom of the conduction band and the top of the valence band of the electrons in a crystalline solid. The forbidden energy gap is calculated for all molecules by the following formula [109,110]:

$$E_{gap}=E_{LUMO}-E_{HOMO} \qquad (2-41)$$

Where E_{gap} is the forbidden energy gap.

E_{LUMO} is the energy of the lowest unoccupied molecular orbital.

E_{HOMO} is the energy of the highest occupied molecular orbital.

2-7-4 Ionization Potential (IP)

The ionization potential (IP) for a molecule is the amount of energy required to remove an electron from an isolated atom or molecule and expressed as the energy difference between the positive charged energy E (+) and the neutral E(n) according to the following relation [111,112]:

$$IP = E(_{+}) - E(_{n}) \qquad (2-42)$$

$$IP = - E_{HOMO} \qquad (2-43)$$

2-7-5 Electron Affinity (EA)

The electron affinity (EA) of a molecule or atom is the energy change when an electron added to the neutral atom to form a negative ion and expressed as the energy difference between the neutral energy E(n) and the negative charged energy E(-) according to the following relation [113-115]:

$$EA = E(_n) - E(_-) \quad (2-44)$$

In molecular orbital (MO) theory with the limitation of Koopman theorem [116,117], the orbital energies of the frontier orbitals are given by:

$$EA = - E_{LUMO} \quad (2-45)$$

A molecule with high chemical potential will accept electrons from a molecule with lower chemical potential.

2-8 Ultraviolet – Visible Spectroscopy

Ultraviolet–visible spectroscopy or ultraviolet-visible spectrophotometry (UV-Vis or UV/Vis) refers to absorption spectroscopy or reflectance spectroscopy in the ultraviolet-visible spectral region. This means that it uses light in the visible and adjacent (near-UV and near-infrared, NIR) ranges. The absorption or reflectance in the visible range directly affects the perceived color of the chemicals involved. In this region of the electromagnetic spectrum, molecules undergo electronic transitions. This technique is complementary to fluorescence spectroscopy, in that fluorescence deals with transitions from the excited state to the ground state, while absorption measures transitions from the ground state to the excited state [118]. When continuous radiation passes through a transparent material, a portion of the radiation may be absorbed. If that occurs, the residual radiation, when it passed through a prism, yields a spectrum with gaps in it, called an absorption spectrum. As a result of energy absorption, atoms or molecules pass from a state of low energy (the initial, or ground state) to a state of higher energy (the exited state) Figure (2.1)

depicts this excitation process, which is quantized. The electromagnetic radiation that is absorbed has energy exactly equal to the energy difference between the excited and ground state.

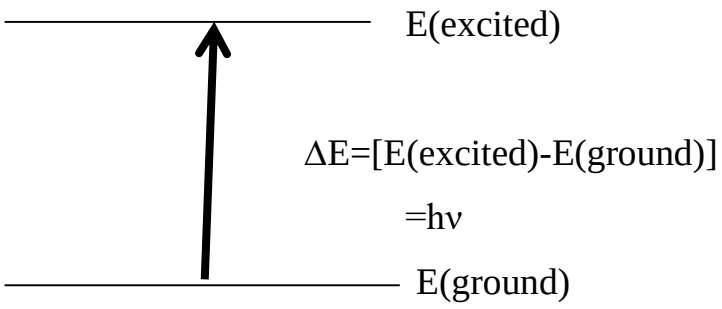

Figure (2.1): The excitation process [118].

In the case of ultraviolet and visible spectroscopy, the transition that results in the absorption of electromagnetic radiation in this region of the spectrum is transition between electronic energy levels. As a molecule absorbs energy, an electron is promoted from an occupied orbital to unoccupied orbital of greater potential energy. Generally, the most probable transition is from the highest occupied molecular orbital (HOMO) to the lowest unoccupied molecular orbital (LUMO).

Chapter Three
Results and Discussion

3-1 Introduction

The present chapter involves the designing pure and doped graphene nano-ribbons by nano tube modular program and calculating their (structural and electronic) properties and UV-Visible using Gaussian View 5.0 software. DFT calculation estimated to compute the ground and excitation proprieties for graphene nano-ribbons at hybrid function B3YLP at basis set 6-31G. Relaxation structure and electronic proprieties were computed at pure state and considerinsit as reference ribbons. After that, placed toxic gas molecule at surface of graphene nano-ribbons, compute relaxation structure and electronic proprieties when toxic gas molecule presence and compared with reference ribbons. The electronic proprieties consist the ionization potential, electron affinity, energy gap, and other important parameter such adsorption energy, sensitivity and optical response. These properties are very essential to determine ability of sensing toxic gas molecule by graphene nano-ribbons. TD-DFT was used to compute optical proprieties.

3-2 First Group

The optimized structures of the graphene nano-ribbons are characterized by the standard orientations (optimized coordinates). Table (3.1) shows the B3LYP/6-31G density functional theory calculations of the optimized parameters of the graphene nano-ribbons structures including the bond length in Angstroms and angles in degrees. Results show that bond length listed in Table (3.1) for relaxation structure has a good agreement with previous study in [119-121].

Table (3.1): B3LYP/6-31G DFT calculations of bond length in Angstroms (Å) and bond angle in degree of the studied graphene nano-ribbons.

Ribbon	*Bond type*	*Bond length (Å)*	*Previous Studies*	*Bond type*	*Angle (Deg.)*	*Previous Studies*
Pure nano-ribbon	C-C	1.446 - 1.465	1.4555[119] 1.461 - 1.537[120]	C⋯C⋯C	118.261 - 123.046	120.232[119] 121.3-131.9[120]
	C=C	1.376 - 1.395	1.3661[119] 1.370[1230	C⋯C–C	117.986 - 122.284	115-121.2[120]
	C⋯C	1.392 - 1.446	1.4305[119] 1.405 - 1.438[120]	H–C⋯C	107.451 - 120.271	120.149 - 119.753[121]
	C-H	1.082 - 1.116	1.0859[119] 1.092[121]	H–C=C	117.978 - 121.933	119.922[119]
				C=C⋯C	120.750 - 122.103	

3-2-1 Ionization Potential (IP) and Electron Affinity (EA) for Pure System

Ionization potential and electron affinity can be described in term of molecular orbital energy using Koopman theory, ionization potential equivalent mines higher occupied molecular orbitals, electron affinity expressed by lowest unoccupied molecular orbitals. Table (3.2) declares the calculations of some electronic variables of the pure graphene nano-ribbons in absence and presence gases molecule measured by electron volt unit in the first group results from the B3LYP/6-31G-DFT calculations. These variables are computed according to Koopmans theorem, and included the ionization potential IP and electron affinity EA in Table (3.2). IP and EA for pure ribbon are (5.097 and 3.367) eV, for gas molecular IP at relaxation

distance have approximately same ability of cation an ion with respect to pure nano-ribbon. That mean electron needs about 5 eV of energy to become cation.

Table (3.2): Represents IP and EA for pure graphene nano-ribbons in the first group.

Ribbon	***IP (eV)***	***EA (eV)***
Pure	5.097	3.367
Pure-NH_3	4.998	3.298
Pure-CO	5.012	3.291
Pure-Br_2	5.237	4.004

3-2-2 Relaxation Distance and Adsorption Energy for Pure System

Three gases were used in this part which are ammonia, bromine and mono carbon oxide gases to study the interaction of them with the surface of graphene nano-ribbon. First step determination full relaxation between gas molecule and a surface of graphene nano-ribbon and determine the energy of stability, besides the type of adsorption at these distances. Table (3.3) shows full relaxation distance and adsorption energy computed by DFT. Figure (3.1) shows full relaxation structure. Results indicate that Br_2 and CO gases molecule have chemical adsorption but NH_3 is physical.

Table (3.3): Adsorption energy and relaxation distance for system under study.

Ribbon	*Adsorption energy (eV)*	*Full relaxation distance(Å)*
Pure-NH_3	-0.272	2.539
Pure-CO	-3.722	1.322
Pure-Br_2	-31.183	2.741

Ribbon	**Structure**
Pure	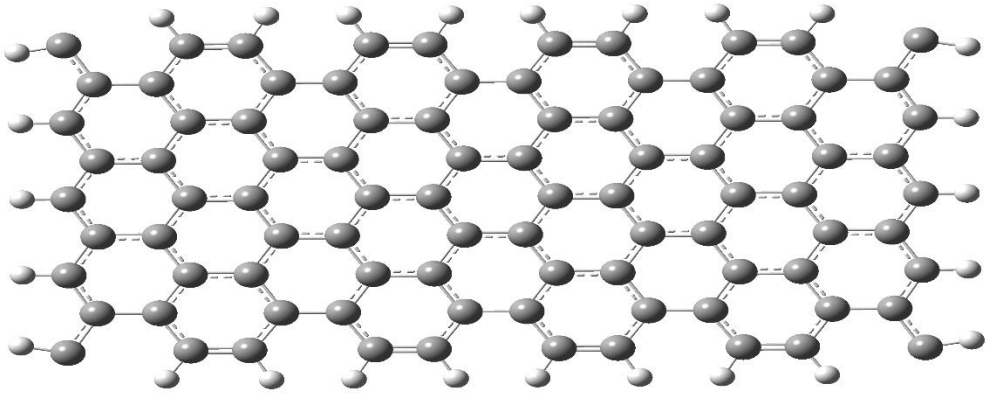
Pure - NH_3	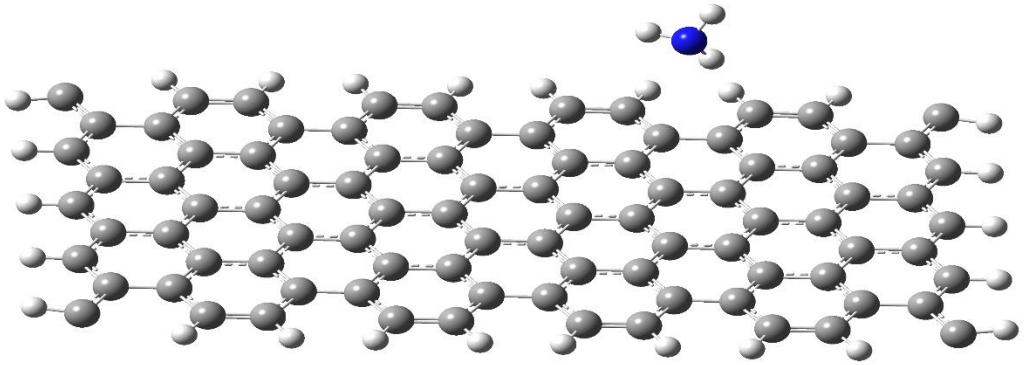

Pure - CO	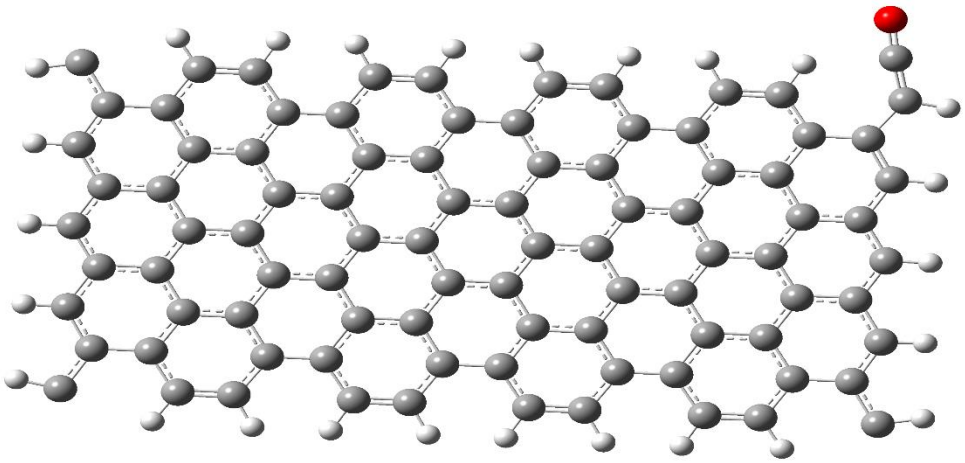
Pure - Br_2	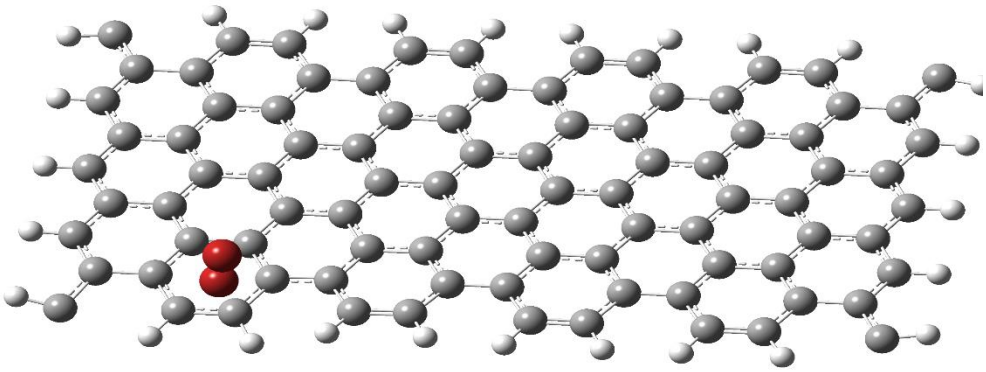

Figure (3.1): Shows full relaxation structure for gas molecule adsorption on graphene surface.

3-2-3 Electronic States and Energy Gap for Pure System

HOMO, LUMO and E_g are important parameters to determine ability of electrons transition and type of materials classification (Conductor, Semiconductor and Insulator). Firstly, energy gap for standard ribbon without gas interaction on surface, energy gap for graphene ribbon is 1.729 eV indicating it as a semiconductor material. Table (3.4) represents HOMO, LUMO and energy gap for adsorption process. HOMO is more essential orbital on the charge transfer consequently always

to graphene. Because of mainly it located on the atom of gas molecule, the charge transfer is the largest when a graphene nano-ribbon interacted with Br_2 gas molecule.

Table (3.4): E_{HOMO}, E_{LUMO} and energy gap in eV for pure graphene nano-ribbons.

Ribbon	***Electronic states***		***Energy Gap(eV)***
	$E_{HOMO}(eV)$	$E_{LUMO}(eV)$	
Pure	-5.097	-3.367	1.729
Pure-NH_3	-4.998	-3.298	1.7
Pure-CO	-5.012	-3.291	1.72
Pure-Br_2	-5.237	-4.004	1.232

Results show that band gap during adsorption process was change and this clear in Br_2 interaction. State of band gap changed from 1.729 to 1.232 eV because high chemical adsorption also it become narrow and high number of electrons transfer through band energy. For NH_3 and CO gas molecules interaction, they have low effect on band gap and transfer of valance electron less than Br_2 gas molecule. Molecular orbital distribution for pure nano-ribbon in Figure (3.2) show that LUMO orbital charge surrounding carbon atoms. HOMO orbital charge distribution around carbon atoms at the edge.

Ribbon	*HOMO*	*LUMO*
Pure	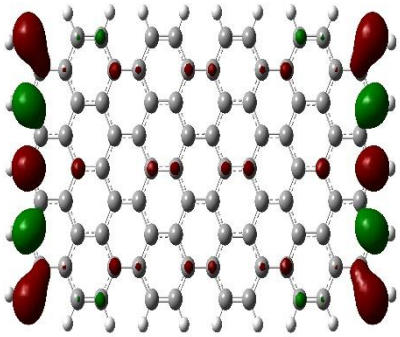	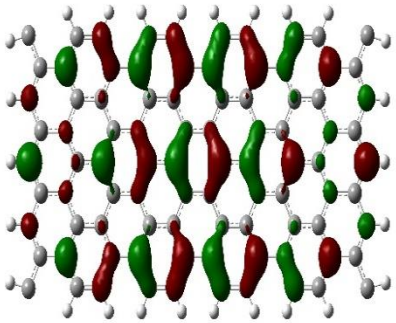
NH_3 - Pure	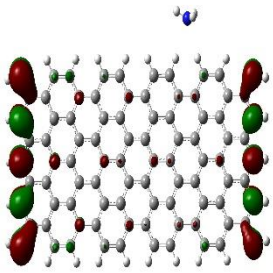	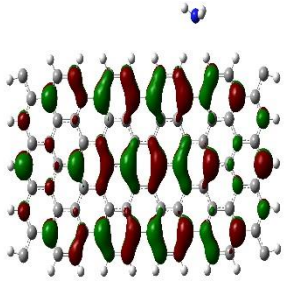
CO- Pure	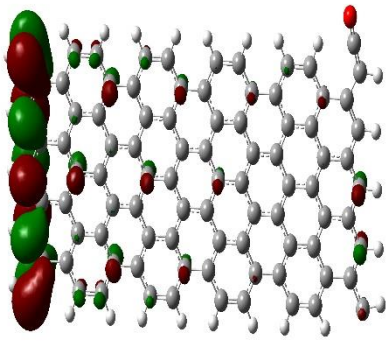	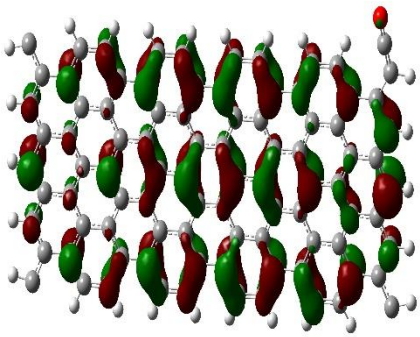
Br_2- Pure	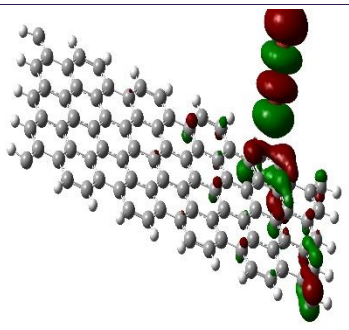	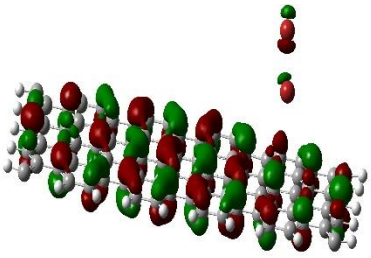

Figure (3.2): Represents HOMO and LUMO charge distribution for adsorption process.

In Frontier orbitals (HOMO and LUMO), at presence gases molecule, for Br_2 gas, because of high chemical adsorption charges distribution is surrounding the molecule and some atoms belong to the surface this clear in HOMO, but for LUMO charge distribution overlap atoms of gas molecule and nano-ribbon. Other gases because of low chemical for CO and physical adsorption for NH3, molecular orbital doesn't affect so that Frontier orbital have same distribution of pure graphene nano-ribbon.

3-2-4 Total Energy and Sensitivity for Pure System

Total energy is a stability of the system, the more energy increases by negative value, the system becomes more stable. Sensitivity of gases that interact with surface of pure graphene nano-ribbon is important tool to checking ability to sense gases. The result of sensitivity shows that in pure system Br_2 more favorite because high chemical adsorption form compared with CO and NH_3 gas molecule. Where the sensitivity can be calculated from the energy gap values according to the equation [$S= (Eg_0-Eg_1)/Eg_0$], where Eg_0 represents the energy gap of nano-ribbon without gas molecules, Eg_1 represents the energy gap of nano-ribbon with gas molecules. The results of sensitivity were agreement with a calculation for an adsorption energy. Table (3-5) represents the total energy and sensitivity in a. u., from this table, we noted that ammonia gas has low energy and sensitivity.

Table (3.5): Represents Total Energy and Sensitivity for pure graphene nano-ribbons.

Ribbon	***E_{total} (a.u.)***	***Sensitivity*100%***
Pure	-3444.48	----
Pure-NH_3	-3501.02	1.683
Pure-CO	-3557.88	0.519
Pure-Br_2	-8587.62	28.755

3-2-5 UV-Visible Spectrum for Pure System

TD-DFT calculation is used to calculate UV spectra at basis set 6-31G and the hybrid function B3YLP. Optical properties calculation for graphene nano-ribbon are important to determine a maximum wavelength of absorption. First, for pure grapheme nano-ribbon maximum wavelength of absorption is (575.4) nm. The results indicate that graphene ribbon absorbed in visible spectra. Figure (3.3) represents UV-Visible spectra for pure ribbon under study. For pure-NH_3 nano-ribbon maximum absorbed wavelength is equal (λ_{NH3}=578.539) nm. Second for Pure-Br_2 nano-ribbon maximum absorbed wavelength is equal (λ_{Br2}=756) nm. Finally, for Pure-CO nano-ribbon maximum absorbed wavelength is equal (λ_{CO} =590) nm. It is clear that the shift in UV-Visible spectram due to high chemical adsorption in Br_2 and CO is very big as compared with NH_3 gas molecule. The results indicate that pure graphene nano-ribbon absorbed in visible spectra and it have red shift.

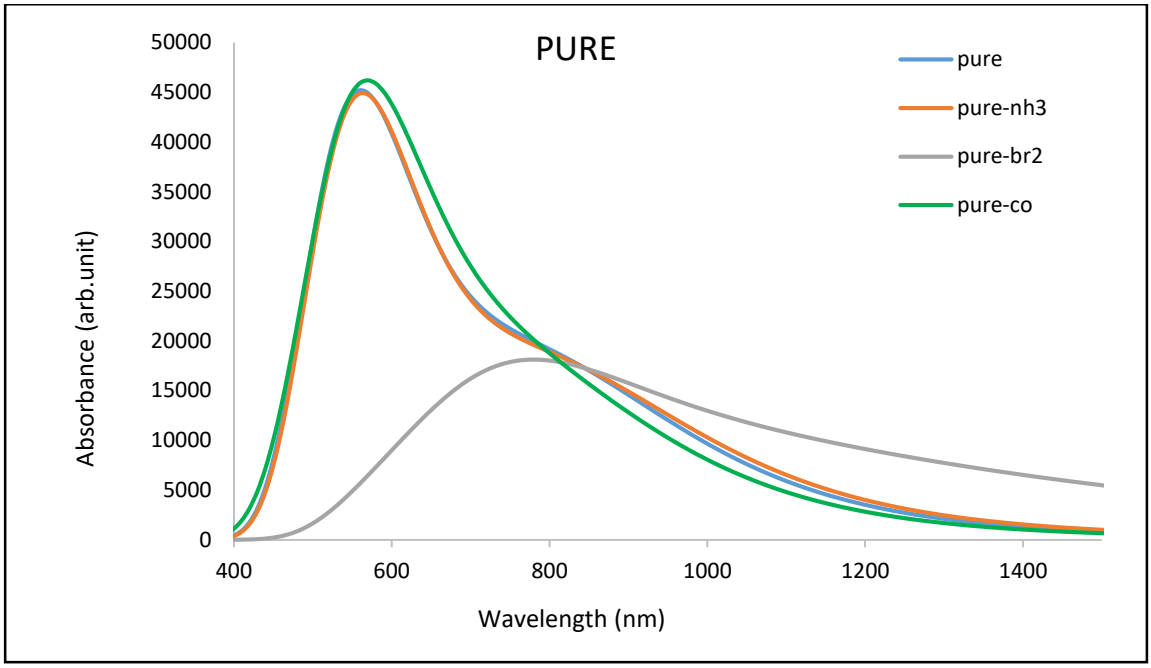

Figure (3.3): Represents UV-Visible spectrum for pure graphene nano-ribbons.

Table (3.6) shows the optical response measurements calculated from the equation [N = $(\lambda_0 - \lambda_{gas})/\lambda_0$], the pure graphene system has a high optical reactivity with Br_2 gas. As for NH_3 gas, it showed a few responses, as the peak of the response was 0.003.

Table (3.6): Represent optical response in pure system.

Nano-ribbon	***Wavelength (nm)***	***Optical response***
Pure	576.4	----
Pure-NH_3	578.539	0.003
Pure-CO	800	0.023
Pure-Br_2	816	0.311

3-3 Second Group

This section investigation the properties graphene nano-ribbons doped with 4 atoms of sulfur with three toxic gases (NH_3, Br_2, CO) interaction with surface. Table (3.7) shows the B3LYP/6-31G density functional theory calculations of the optimized parameters of the doped graphene nano-ribbon structures including the bond length in Angstroms and angles in degrees. Table (3.7) show that the bond length which are (C=C), (C-C), (C⋮⋮C), (C-H) and (C=S) . Also angles are C⋮⋮C–C, H–C⋮⋮C, C⋮⋮C⋮⋮C, H–C=C and C=C⋮⋮C bonds are in the same ranges of aromatic carbon rings. The result showed that was a good relaxation structure for all bond that formed nano system.

Table (3.7): B3LYP/6-31G-DFT calculations of bond length in Angstroms (Å) and angles in degree of the studied S-doped graphene nano-ribbons.

Ribbon	*Bond type*	*Bond length (Å)*	*Bond type*	*Angle (Deg.)*
4S-doped nano-ribbon	C-C	1.455 - 1.481	C⋯C⋯C	106.950 - 144.668
	C=C	1.361	C⋯C–C	115.293 - 124.604
	C⋯C	1.387 - 1.445	C⋯C–S	106.805 - 116.064
	C-H	1.076 - 1.103	C=C–S	114.800
	C=S	1.518 - 1.590	C⋯C–H	108.399 - 120.900
			C=C–H	116.967 – 119.564
			C⋯C=C	121.917 – 134.799
			C–C=C	111.444
			C–C–C	126.203
			C–S–C	117.706 – 122.363

3-3-1 Ionization Potential (IP) and Electron Affinity (EA) for S Doped System

In this section investigation IP and EA for graphene nano-ribbon doped with four sulfur atom in absence and presence of gases molecules measured in unit of eV. Table (3.8) declares the calculations of IP and EA for doped graphene nano-ribbons at basis set 6-31G and hybrid function B3LYP. IP and EA for graphene S-doped nano-ribbon 5.932 and 1.791 eV, respectively. Results of IP show that all interacted systems have high ability for cation electron varies between (4.841 - 5.017) eV, in other hand adsorption process modified an ion process due to high chemical an adsorption for all systems.

Table (3.8): Represents IP and EA for S-doped graphene nano-ribbons in eV.

Ribbon	*Ionization Potential (IP)*	*Electron Affinity (EA)*
4S	5.932	1.791
4S-NH_3	4.971	3.560
4S-CO	5.017	3.603
4S-Br_2	4.841	3.865

3-3-2 Relaxation Distance and Adsorption Energy for S-Doped System

NH_3, Br_2 and CO gases that interact with doped graphene nano-ribbon. The first step of determination the full relaxation between gas molecule and doped graphene nano-ribbon and determine energy of stability, as well as the type of adsorption at relaxation distances. Table (3.9) shows full relaxation distance and adsorption energy computed by DFT. Result showed that doped by S atom modified an adsorption energy for all gases and this clears for NH_3, it is changed from physical to chemical interaction. Also doped mechanism increased a chemical adsorption for Br_2 and CO gases and become nano system more sensitive for them. Other mechanism that modify an adsorption process is defect that appear one from doped method and other during interaction between gases molecule and surface of doped nano-ribbon. Figure (3.4) shows full relaxation structure for gas molecule adsorption on S doped graphene surface are NH_3, Br_2 and CO, respectively. Figure (3.4) represents most geometrical orientation between gas molecule and surface S-doped nano-ribbon.

Table (3.9): Adsorption energy and relaxation distance for system under study.

Ribbon	***E_{ad} (eV)***	***Full relaxation distance(Å)***
4S-NH_3	-30.073	2.295
4S-CO	-30.286	2.656
4S-Br_2	-40.468	2.952

Ribbon	**Structure**
4S	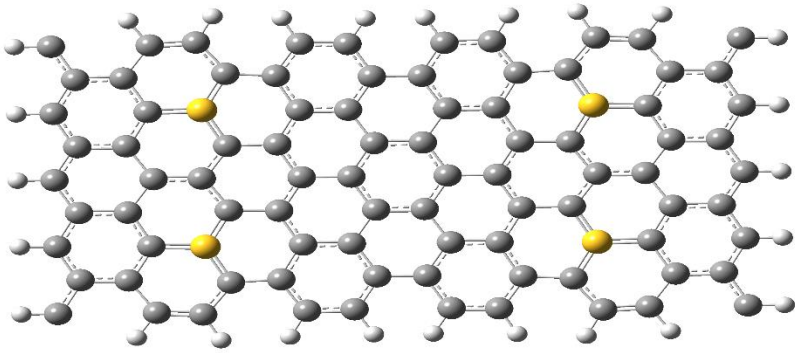
4S-NH₃	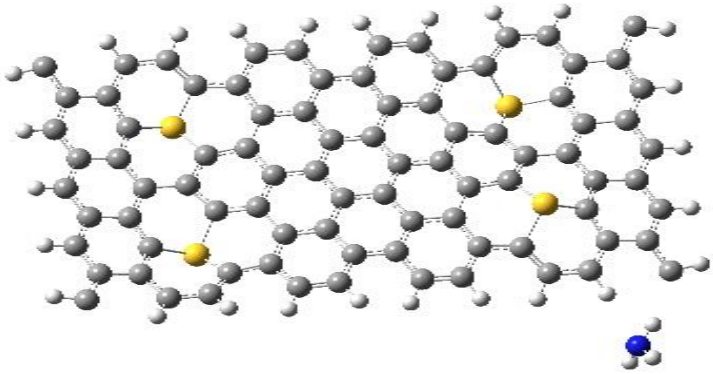
4S-CO	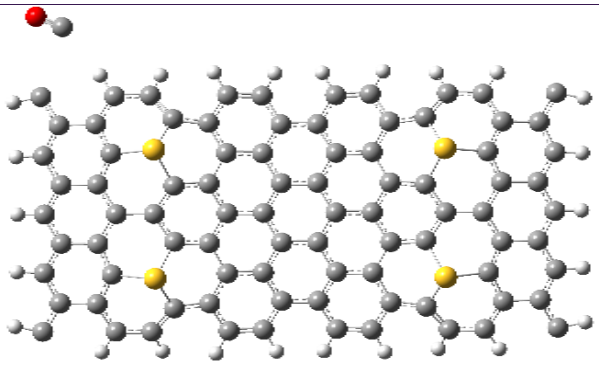

4S-Br₂	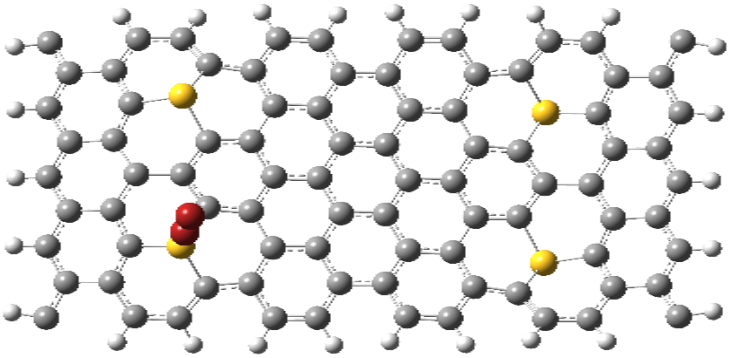

Figure (3.4): Shows full relaxation structure for gas molecule adsorption on S-doped graphene surface NH_3, Br_2 and CO, respectively.

3-3-3 Electronic States and Energy Gap for S-Doped System

HOMO, LUMO and Energy Gap (E_g) are important parameters to determine the ability of electrons transition and the type of materials classification (Conductor, Semiconductor and Insulator). Energy gap for S-doped nano-ribbon without gas interaction on surface is 4.1409 eV as a semiconductor material. For doped graphene nano-ribbon HOMO distribution around C-C bonding, LUMO located around S and some carbon atoms. Tables (3.10) represent HOMO, LUMO and energy gap for adsorption process. Result shows that all molecular orbitals are shifted to lower energy due to high chemical adsorption for all gases interaction on the surface. Band gap changed due to molecular orbital shifting, it varies in range (0.97-1.414) eV in other hand increasing conductivity of nano-system. Reducing in energy gap a clear reason of transfer high amount of valance electron.

Table (3.10): E_{HOMO} , E_{LUMO} and energy gap in eV of the S-doped graphene nano-ribbons.

Ribbon	*Electronic states*		*Energy Gap (eV)*
	$E_{HOMO}(eV)$	E_{LUMO} *(eV)*	
4S	-5.932	-1.791	4.140
4S- NH_3	-4.971	-3.560	1.410
4S- CO	-5.017	-3.603	1.414
4S- Br_2	-4.841	-3.865	0.976

HOMO and LUMO level during adsorption process was changed due to the reactivity between gases molecules and surface of S-doped graphene nano-ribbon. HOMO level during adsorption process was increasing for all gases, but LUMO is reverse from HOMO. Band gap state according to change of molecular orbitals will be effected. Because chemical adsorption between all gases and surface of doped graphene nano-ribbon state of energy gap was changed. Energy gap values during adsorption mechanism varies from 0.97 to 1.41 eV this result show that band gap become very narrow as compared with pure system that interacts with same gases and permission to high number of valance electron transfer through it. Figure (3.5) represent HOMO and LUMO charge distribution for adsorption systems.

Ribbon	*HOMO*	*LUMO*
4S	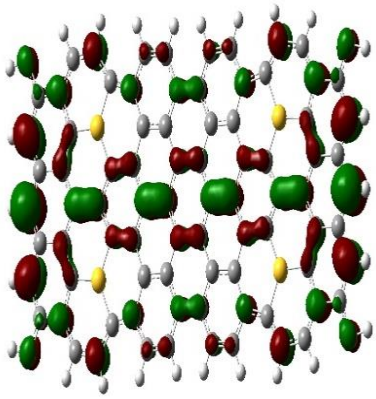	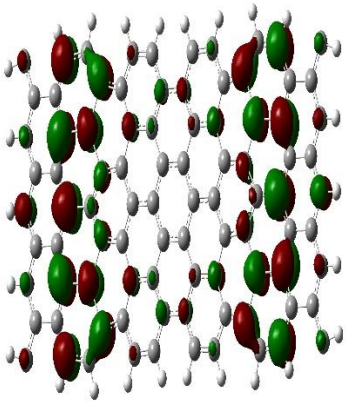
4S-NH_3	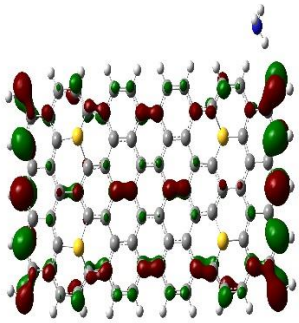	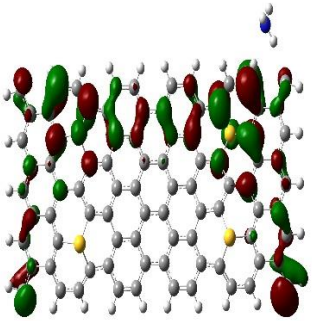
4S-CO	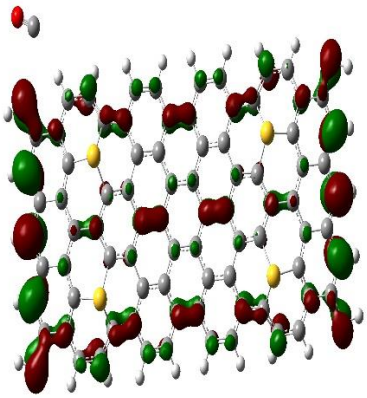	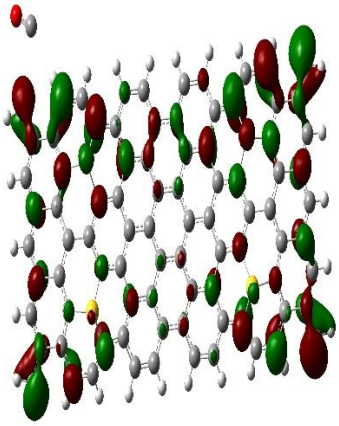

4S-Br₂	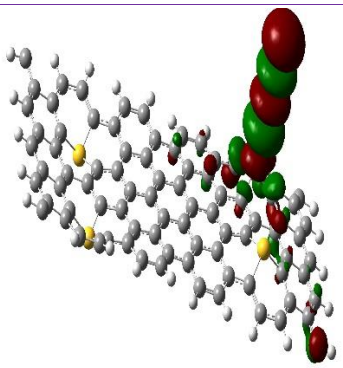	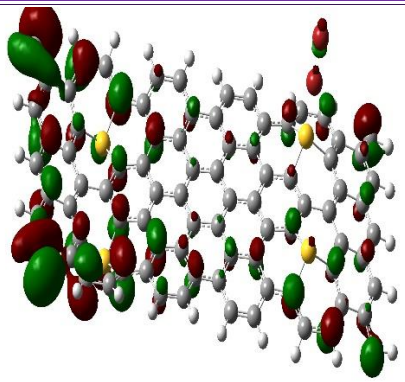

Figure (3.5): Represents HOMO and LUMO distribution for adsorption systems.

3-3-4 Total Energy and Sensitivity for S-Doped System

In this section, we investigation sensitivity of S-doped nano-ribbon that interaction with gases molecule as a function of energy gap, the result of sensitivity listed in Table (3.11). Results showed that the sensitivity of gases were modified as compared with pure nano-ribbon. Sensitivity of gases arranged as $Br_2 > NH_3 \cong CO$, increasing in ability of sense due to high chemical adsorption raised during interaction between gases molecule and surface of S-doped nano-ribbon. The result showed that also, sensitivity calculation was in agreement with the arrangement of an adsorption energy.

Table (3.11): Represents Total Energy and Sensitivity.

Ribbon	***E_{total} (a.u.)***	***Sensitivity * 100%***
4S	10477	----
4S-NH_3	-4941.32	65.928
4S-CO	-4998.05	65.843
4S-Br_2	-10027.2	76.429

3-3-5 UV-Visible Spectrum for S-Doped System

Optical properties calculation for S-doped graphene nano-ribbon were important to determine a maximum wavelength of absorption. Table (3.12) listed the values of maximum wavelength of absorption in nm unit. Resulting from high chemical adsorption for all gases interacted with surface the spectrum was changed. The result show that all system has blue shifting in the electromagnetic radiation and Br_2 has high excitation energy as compared with other gases. Figure (3.6) represents UV-Visible spectram for doped graphene nano-ribbons under study.

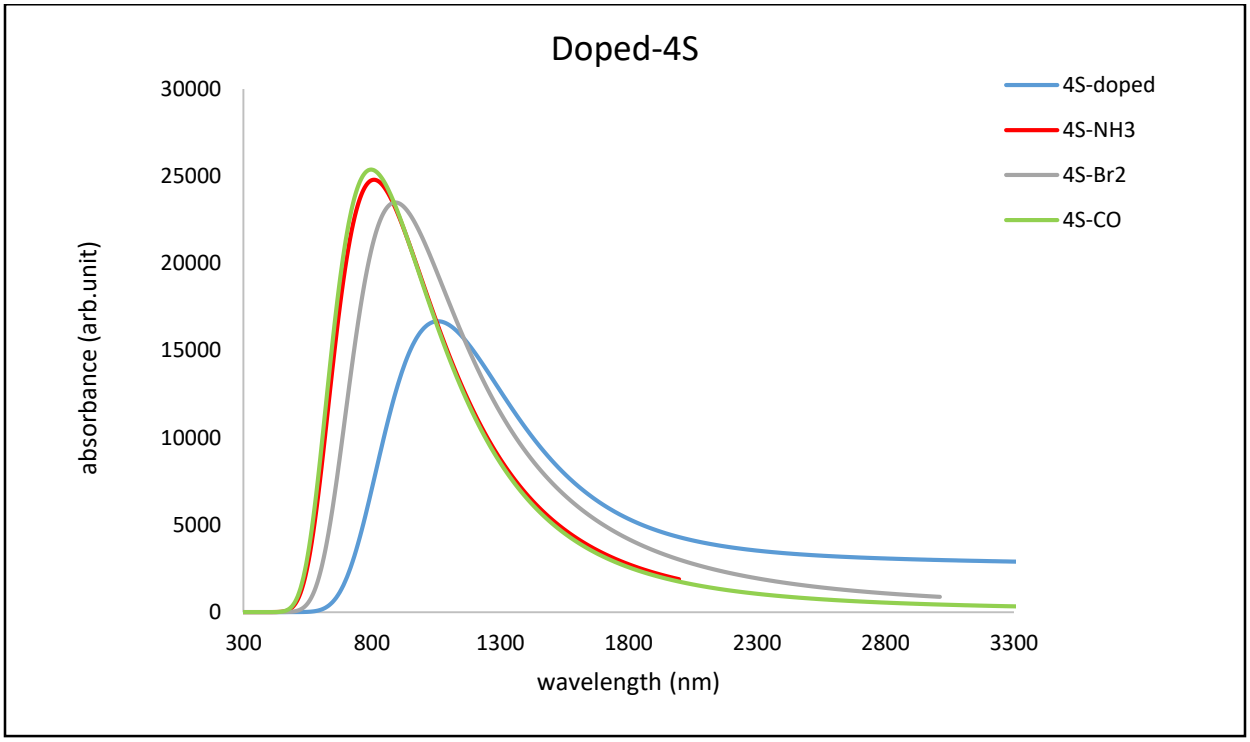

Figure (3.6): Represents UV-Visible spectram for S-doped graphene nano-ribbons under study.

The results showed that each of NH_3 and Br_2 gas has a good optical response compared to CO gas, which showed very little optical reactivity, as in Table (3.12).

Table (3.12): Represents optical response in S-doped system.

Nano-ribbon	***Wavelength (nm)***	***Optical response***
4S	1079.998	----
4S-NH_3	760.963	0.295
4S-CO	1056	0.022
4S-Br_2	573.096	0.469

3-4 Third Group

This section investigation the properties graphene nano-ribbons doped with 4 atoms of aluminum with the same three toxic gases (NH_3, Br_2, CO) that interact with a surface. Table (3.13) shows the B3LYP/6-31G density functional theory calculations of the optimized parameters of the Al-doped graphene nano-ribbon structures including the bond length in Angstroms and angles in degrees. From Table (3.13) it is clear that the bond which are (C=C), (C-C), (C⋮⋮C), (C-H) and (C-Al), also, angles are C⋮⋮C–C, H–C⋮⋮C, C⋮⋮C⋮⋮C, H–C=C, C=Al=C, C=Al–C, C–C–Al, C⋮⋮C=Al and C=C⋮⋮C bonds are in the same ranges of aromatic carbon rings. Result show that is a good relaxation structure for all bonds that formed nano system.

Table (3.13): B3LYP/6-31G-DFT calculations of bond length in Angstroms (Å) and bond angle in degree of Al-doped graphene nano-ribbons.

Ribbon	*Bond type*	*Bond length (Å)*	*Bond type*	*Angle (Deg.)*
4Al-doped nano-ribbon	C-C	1.423 – 1.642	C‴C‴C	109.748 – 128.655
	C=C	1.348	C‴C–C	113.393 – 133.8191
	C‴C	1.399 – 1.440	H–C‴C	108.024 – 120.222
	C-H	1.073 – 1.114	H–C=C	116.980 – 119.576
	C=Al	1.775 – 1.790	H–C–C	111.208 – 121.758
	C-Al	1.795	C=C‴C	131.334
			C–C=C	115.092 – 145.183
			C=Al=C	116.316
			C=Al–C	119.273 – 124.410
			C‴C=Al	113.803 – 117.696
			C–C–Al	105.530

3-4-1 Ionization Potential (IP) and Electron Affinity (EA) for Al-Doped System

In this section investigation IP and EA for graphene nano-ribbon doped with 4 Al atoms in absence and presence gases molecules measured in eV, also study effect of gases on them. Table (3.14) declares the calculations of IP and EA for doped graphene nano-ribbons at basis set 6-31G and hybrid function B3LYP. IP and EA for graphene Al-doped nano-ribbon are 5.321 and 4.404 eV, respectively. Result showed that all interaction due to high chemical an adsorption system has high ability to cation electron varies between (4.95 - 5.32) eV, in other hand adsorption process modified an ion process.

Table (3.14): Represents IP and EA of the Al-doped graphene nano-ribbons.

Ribbon	*Ionization Potential (IP)*	*Electron Affinity (EA)*
4Al	5.321	4.404
4Al-NH_3	4.959	4.065
4Al-CO	5.115	4.190
4Al-Br_2	5.315	4.517

3-4-2 Relaxation Distance and Adsorption Energy for Al-Doped System

In this part, we investigation adsorption process between selected gases molecule in our study and surface of Al-doped nano-ribbon. Table (3-15) show full relaxation distance and adsorption energy computed by DFT. Figure (3.7) shows full relaxation structure. Results show that NH_3 and CO gases molecule have low chemical adsorption -4.97 and -4.15 eV, respectively. Br_2 adsorption energy was very high chemical interaction compared with two past gases. Adsorption of Br_2 gas molecule that interacted with the surface of Al-doped nano-ribbon gave an iterance to physics high energy. Modified of adsorption energy in this section resulting from two mechanisms one is doped by metal atom and another is appearing of defected during interaction process.

Table (3.15): Adsorption energy and relaxation distance for Al-doped nano-ribbons.

Ribbons	***Adsorption energy***	***Full relaxation distance(Å)***
4Al-NH_3	-4.979	2.043
4Al-CO	-4.157	2.126
4Al-Br_2	-171.048	2.496

Ribbon	Structure
4Al	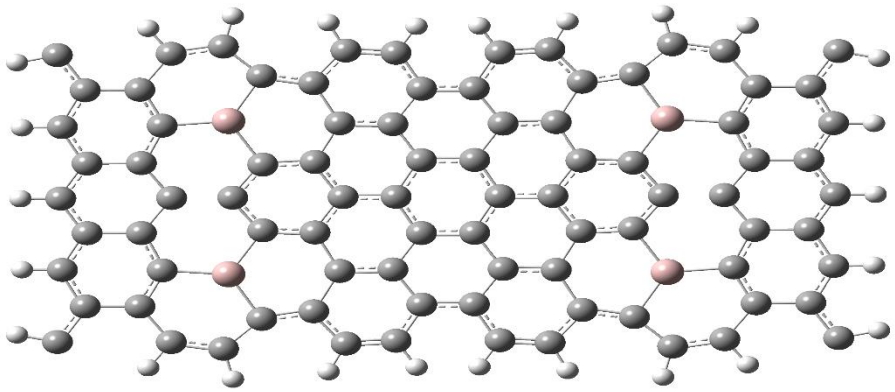
4Al- ***NH_3***	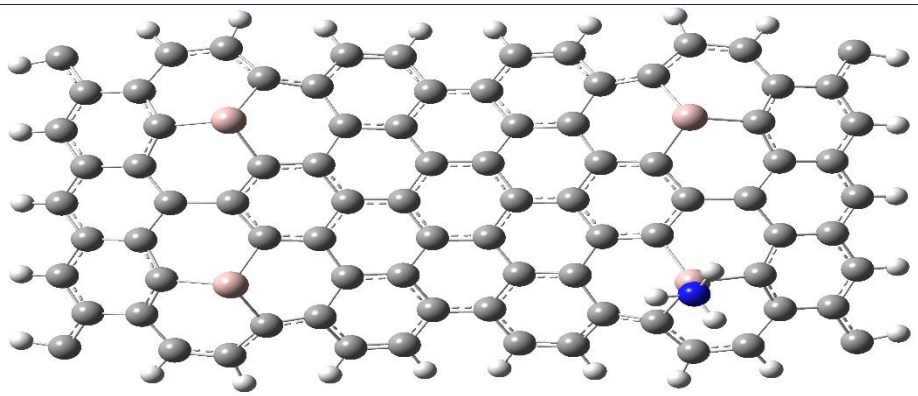
4Al- ***CO***	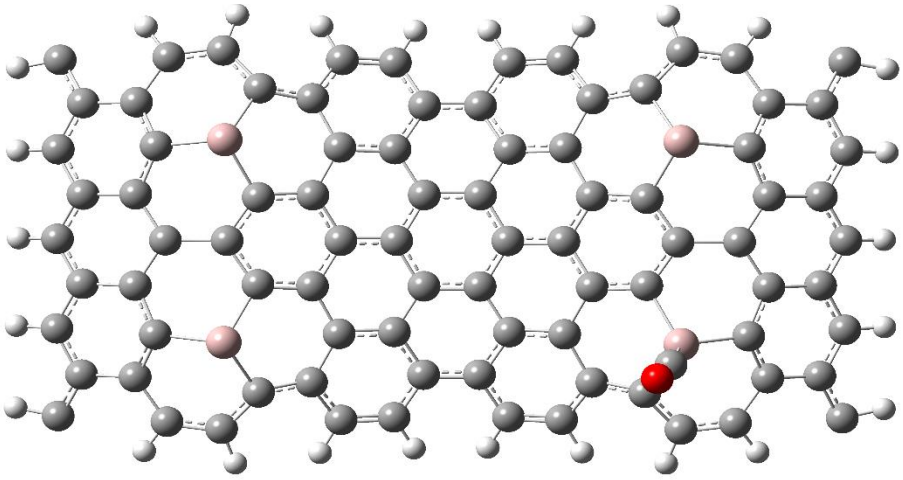

4Al- *Br_2*	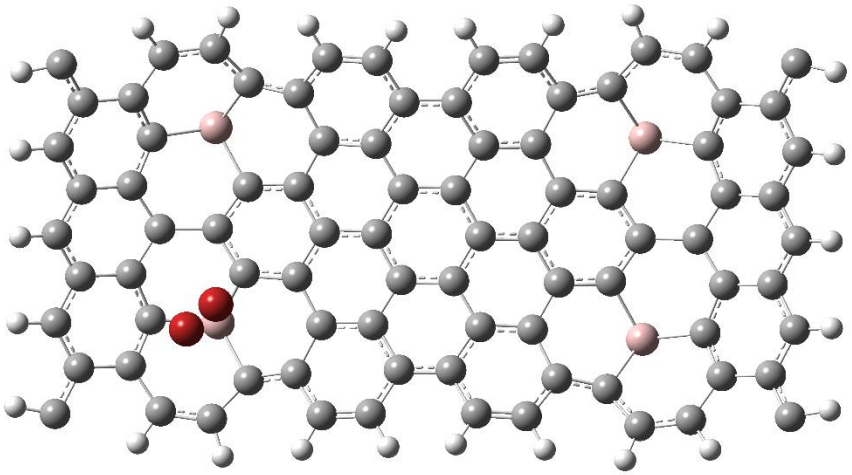

Figure (3.7): Shows full relaxation structure for gas molecule adsorption on Al doped graphene surface are NH_3, Br_2 and CO respectively.

3-4-3 Electronic States and Energy Gap for Al-Doped System

In this section we study the effect of adsorbed gases molecule on HOMO, LUMO and E_g that interacted with surface of Al-doped nano-ribbon. Figure (3.8) represents molecular orbital distribution for Al-doped nano-ribbon in absence and present gases molecules under study. From the Figure (3.8) notes the distribution of the charge of Al-doped nano-ribbon atoms was surrounding doped atoms, which indicate that most of charge is centered around the aluminum atoms. In the case of the reaction of the ammonia gas molecule, from resulting of chemical reaction, we observed a HOMO charges distribution surrounding the aluminum atoms closed to the ammonia gas. For LUMO, most of the charge is distribution on carbon and aluminum atoms far from surface and gas molecule. In the case of CO gas molecule reaction, the distribution of HOMO is almost similar to NH_3 with the concentration of small portion of charges on the gas molecule. While in LUMO, electrons are distributed symmetrically to most of atoms, most of charge are located on the Al atoms. The similarity of distribution behavior that the calculated adsorption energies

of molecules NH_3 and CO have approximately equal values. For bromine gas molecule, we observed a HOMO energy, results show that a charge is mostly centered on the Al atom close to reactive gas on the surface. The remainder of the charge is distributed on the edges of nanoribbon. Whereas in LUMO most of the charges are surrounded by Al atoms in a greater concentration than other atoms. Some of charge is centered on gas molecule. The charge distribution is a result of the very high adsorption energy release compared to NH_3 and CO gases. Distribution of electrostatic charge play an important role in conductivity of nano-systems.

The energy gap considered as an important factor to prove the sensitivity so that any changes on it is a sign of sense process. All computed values of energy gap for aluminum doped graphene nanoribbon were changed. Obvious change of energy gap appears in Br_2 adsorption. For CO adsorption band gap becomes very wide in nanoribbon resulting from high binding system. Table (3-16) shows HOMO, LUMO and energy gap measured in eV unit.

Ribbon	*HOMO*	*LUMO*
4Al	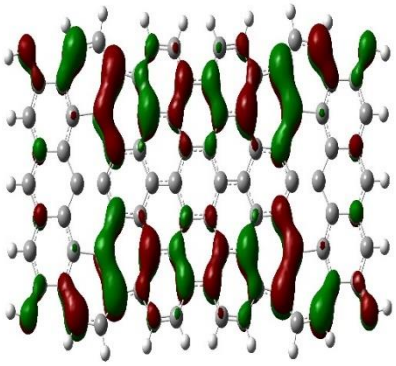	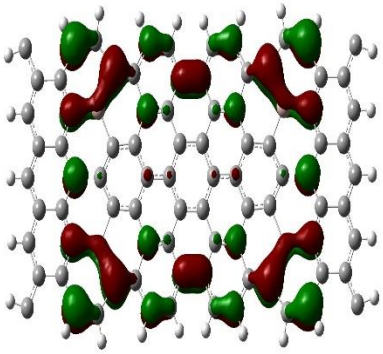
NH_3-4Al	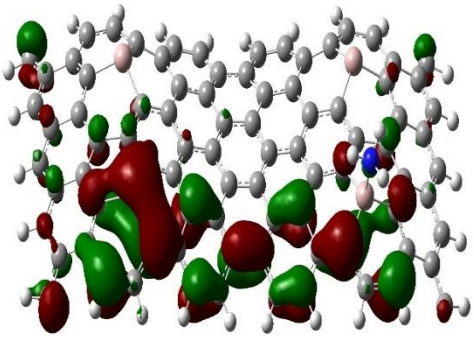	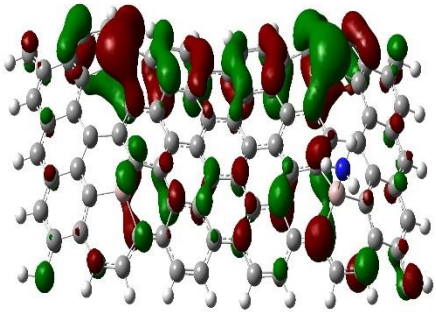
CO-4Al	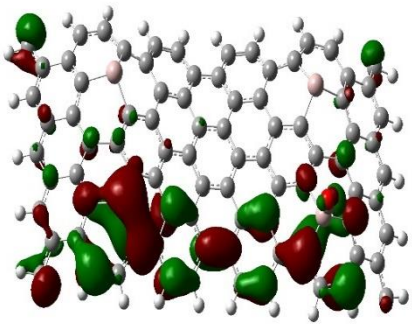	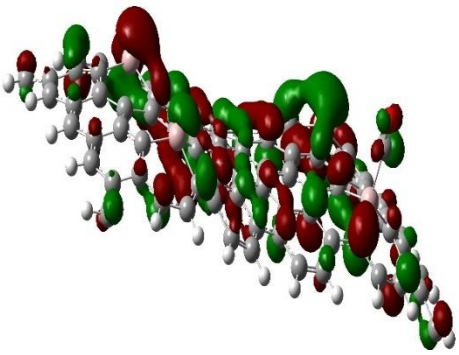
Br_2-4Al	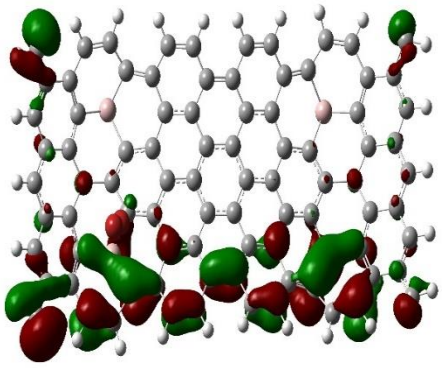	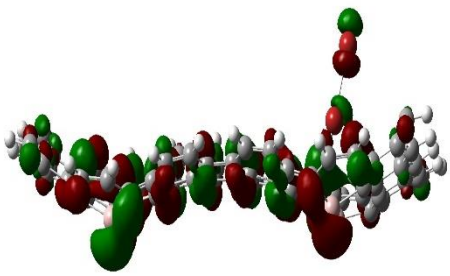

Figure (3.8): Represent molecular orbital distribution for Al-doped nano-ribbons.

Table (3.16): Represents HOMO, LOMO and Energy Gap value in eV of doped Al graphene nano-ribbons.

Ribbon	*HOMO (eV)*	*LUMO (eV)*	*Energy Gap (eV)*
4Al	-5.320	-4.404	0.916
4Al-NH_3	-4.959	-4.065	0.894
4Al-CO	-5.115	-4.190	0.924
4Al-Br_2	-5.315	-4.517	0.798

3-4-4 Total Energy and Sensitivity for Al-Doped System

Sensitivity of gases that interact with surface of Al-doped nano-ribbon, arranged as follow Br_2>NH_3>CO. This result showed that sensitivity of the studied systems is in agreement with adsorption calculations. Br_2 was the highest sensitivity as compared with other gases due to high reactivity of it with respect to NH_3 and CO. Table (3.17) represents total energy and sensitivity.

Table (3.17): Represents total energy and Sensitivity.

Ribbon	*E_{total} a.u.*	*Sensitivity * 100%*
4Al	-4261.7	----
4Al-NH_3	-4318.41	2.434
4Al-CO	-4375.11	0.920
4Al-Br_2	-9409.98	12.915

3-4-5 UV-Visible Spectrum for Al-Doped System

In this part, we study the effect of gases molecule under study on UV-Visible spectrum, and determine types of shifting depending on interactions on the surface of Al-doped nano-ribbon. Figure (3.9) represents UV-Visible spectra for Al doped graphene nanoribbon. The system is in stable state, during the interaction between gas molecule and AL-doping nanoribbon the maximum wavelength was calculated (λ_{4Al} = 864, $\lambda_{4Al\text{-}NH3}$ =1696, $\lambda_{4Al\text{-}Br2}$ = 980, $\lambda_{4Al\text{-}CO}$ =972) nm. Bromine gas absorbs at a wavelength about 980 nm that required for its transition from HOMO to LUMO, which results in strong interaction types $\pi \rightarrow \pi^*$ this case is similar to CO gas with a lower wavelength. The energy released when NH_3 gas interaction is the result of the absorption of wavelength, which leads to release low energy in mid infrared region. Results show that all interacted systems have red shift in electromagnetic radiation, in other hand electrons need a small amount of energy to transport from HOMO to LUMO.

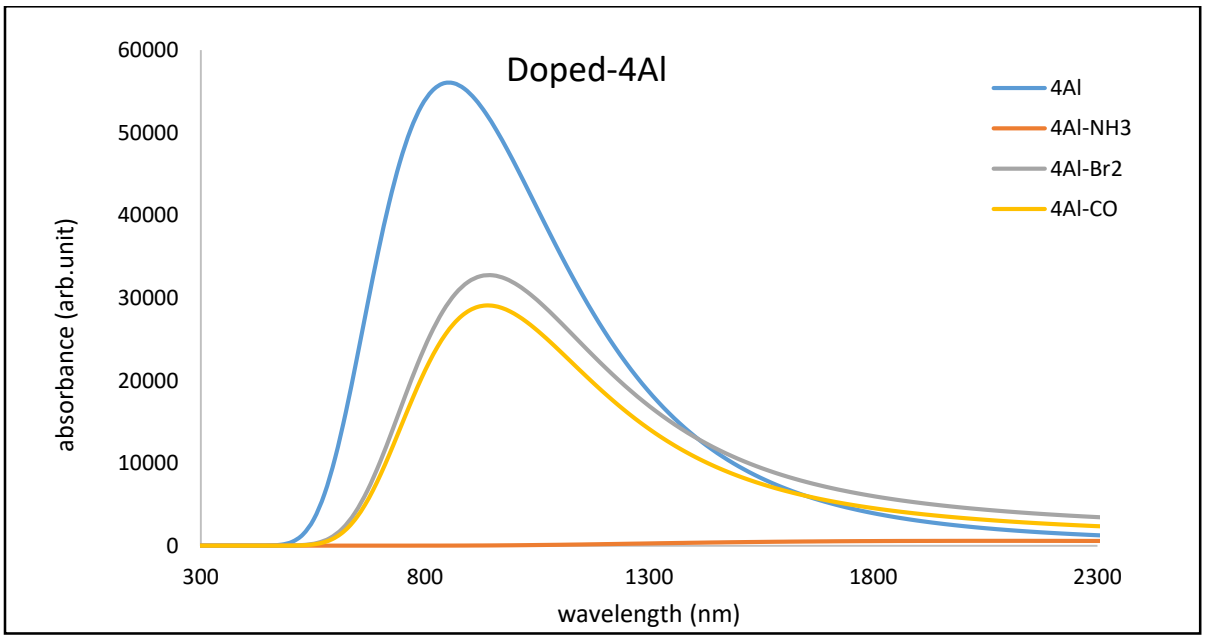

Figure (3.9): Represents UV-Visible spectrum for ribbons under study.

Through Table (3.18) the measurements revealed an ideal interaction between the NH_3 molecule and the surface of the Al-doped graphene, where the optical response reached 96%. As for Br_2 and CO molecule gas, their reactivity is low compared to NH_3 gas.

Table (3.18): Represent optical response in Al-doped system.

Nano-ribbon	***Wavelength (nm)***	***Optical response***
4Al	864	----
4Al-NH_3	1696	0.962
4Al-CO	972	0.125
4Al-Br_2	980	0.134

3-5 Experimental Part

In this part, we explained the thin film preparation mechanism of preparation thin film, solution preparation and formation of graphene (G), aluminum (Al) and doped films (G-Al), where the glass coating technique was used. This section includes a description of all the tools that used in this work. The following is a discussion about optical properties inspection. Figure (3.10) is the schematic diagram of the experimental work.

Thin film technology has revolutionized the field of optics, electronics and magnetism, considering the new and improved optics, electronics, magnetic devices, solar cell and photovoltaics etc. The advantage of thin film devices is low material consumption.

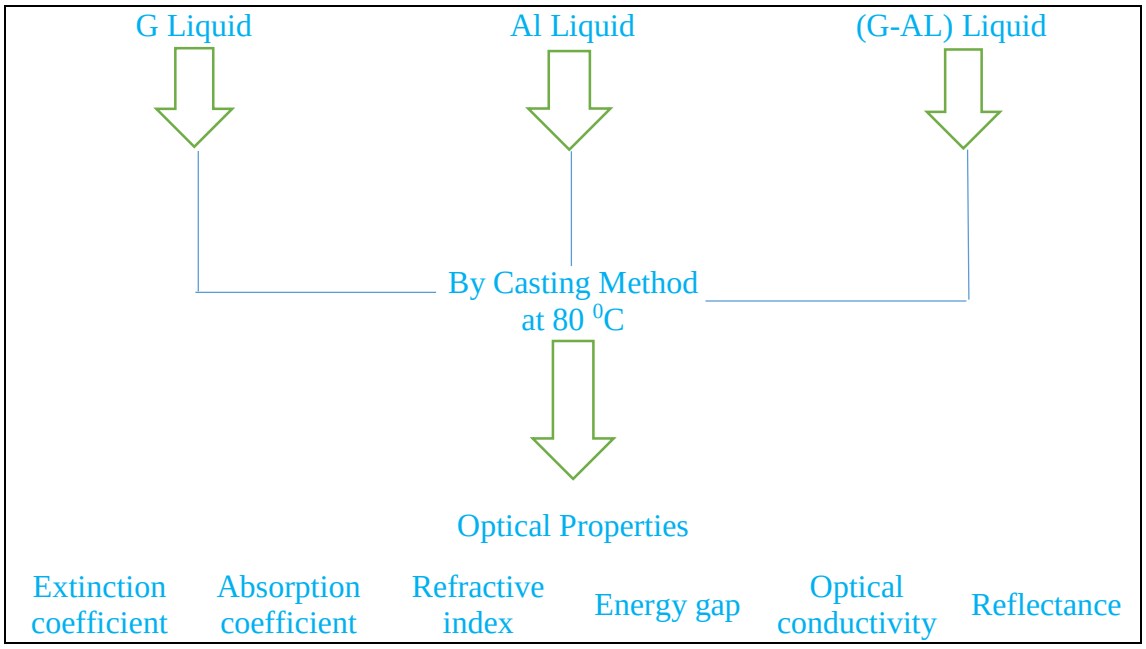

Figure (3.10): Schematic diagram of the experimental work.

3-5-1 Substrate Preparation

Type and nature of the substrate are the influence parameters and have the most important effects on the properties of the deposited films. One type of substrates was used in this study, glass slides which were used to study optical properties of (G, Al, G-Al) thin films.

First step, we cut the glass slides and cleaning, the substrate used for deposits (G, Al, G-Al) thin films in this work is a microscopic glass slides. These glass slides substrates (2.5) cm^2 with 1 mm thickness were subjected to the following steps:

1- The substrates were cleaned by water and a detergent solution to remove any oil or dust that might be on their surface.

2- The substrates were immersed in a clean beaker containing distilled water.

3- Then, the glass substrates were dried and were wiped with soft paper.

Thin films were prepared through the following procedures in the graduate laboratory at Al-Qasim Green University:

A: The pure graphene film was prepared by mixing (0.1 g) of graphene with (25 ml) of distilled water in a beaker until the solution became homogeneous. In the same way and quantities, a pure aluminum film was prepared, the process was carried out at room temperature.

B: Doped graphene nano-ribbons with aluminum was prepared, where (0.05 g) of aluminum was mixed with the same amount of graphene.

Then, the casting method was used to prepare films from these mixtures, as each of these ratios was poured onto petri dish placed on a horizontal surface after balancing it by means of a leveling scale after they were cleaned well several times with distilled water. Under a temperature of 80 ^0C for 30 minutes, this method was

used to get rid of distilled water and get only the materials. A small proportion are added to obtain a thin film thickness.

3-5-2 Optical Measurements

A double–beam UV-Vis 1800 shimadzu spectrophotometer was used to measure the absorption of (G, Al and G-Al) thin films. The background correction is taken for each scan. The transmittance and reflectance data can be used to calculate absorption coefficients of the films at different wavelength which have been used to determine the energy gap Eg. This device is present in Department of Physics / College of Education for Pure Sciences / University of Babylon.

The properties were studied in optical measurements:

1- absorbance
2- transmitance
3- reflectance
4- absorption coefficient
5- extenction coefficient
6- refractive index
7- optical conductivity
8- energy gap

Below is an explanation of these characteristics:

1) Absorbance (A) and Absorption Coefficient (α):

Graphene is stable for all wavelengths, from Figure (3.11 a), it was noticed that there is no change opposite to the aluminum strip and the graphene nano-ribbons has a sudden descent at the wavelength of 340 nm. It was noticed from Figure (3.11 b) the absorbance decreases with the increase in the proportion of (Al) because it is

reflective, From Figure (3.11 c), it was noticed that the value of α is more than 10^4, which means that the energy gap is direct.

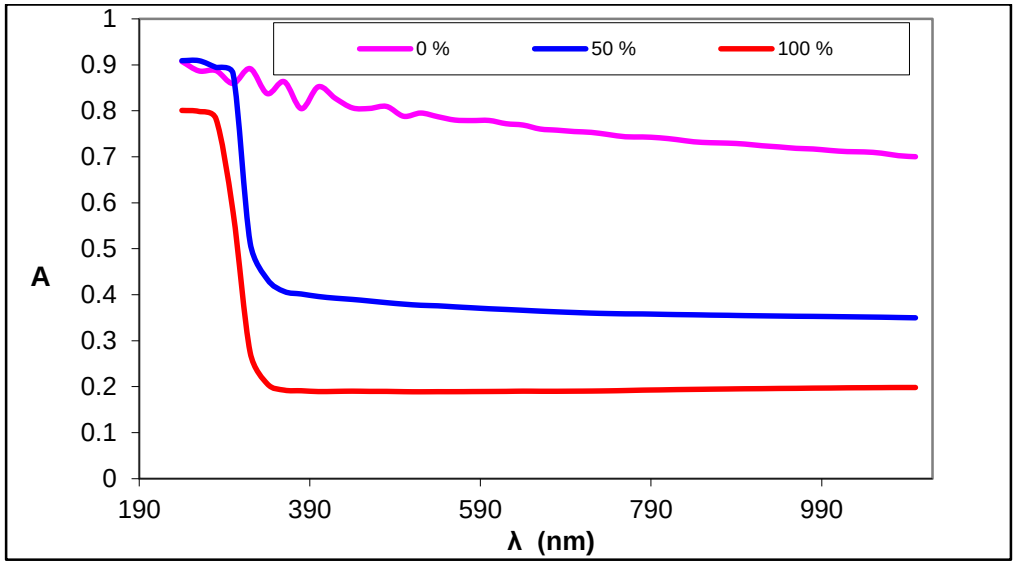

(a)

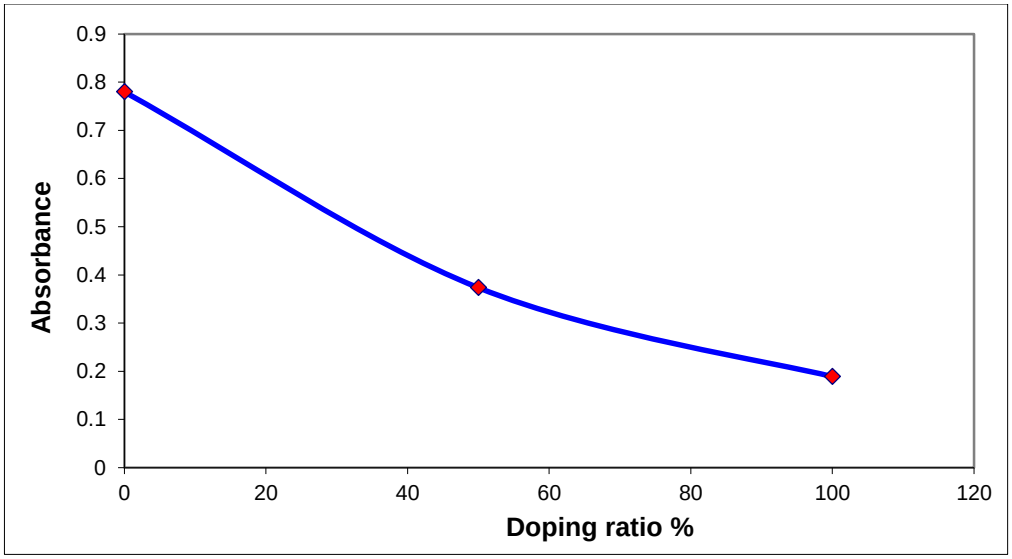

(b)

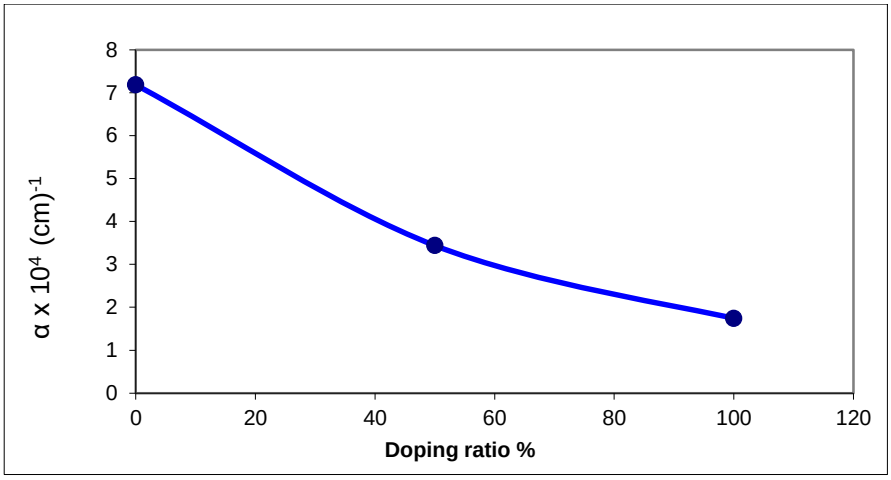

(c)

Figure (3.11): (a) Represents the absorbance of each individual sample. (b) Absorbance chart for all samples together. (c) Absorbance coefficient.

2) Transmitance (T) and Reflectance (R):

The transmittance is opposite absorbance (higher transmittance is lower absorbance) where Al has the highest transmittance and graphene less. Figure (3.12 a) transmittance of samples used.

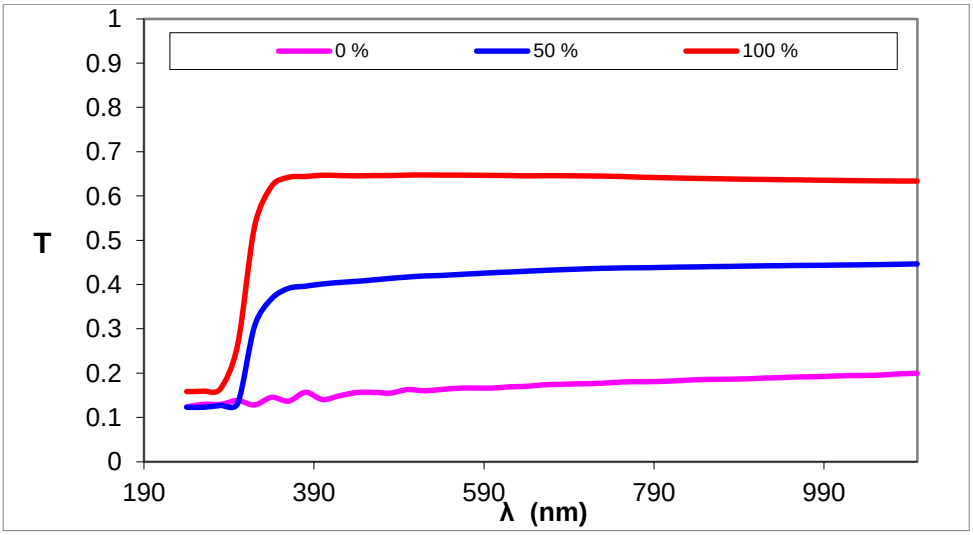

Figure (3.12): Transmittance of samples used.

As for the reflectance, it was noticed here a difference as the doping tape has the highest reflectivity because aluminum is also a reflective material. Figure (3.13) shows the reflectance of the samples.

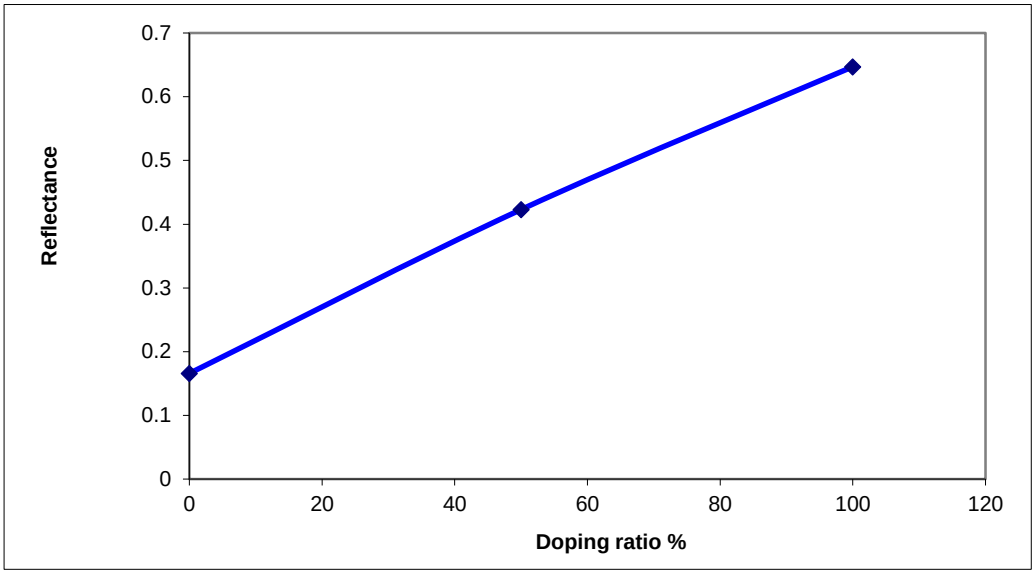

Figure (3.13): Reflectance of the samples.

3) Extenction Coefficient (k) and Refractive Index (n):

The attenuation coefficient (k) as it behaves the same as α behavior decreases with increasing Al as in Figure (3.14 a) the refractive index has a maximum value for the reflectivity, Figure (3.14 b) represents the refractive index. Table (3.19) represents the value of K and n.

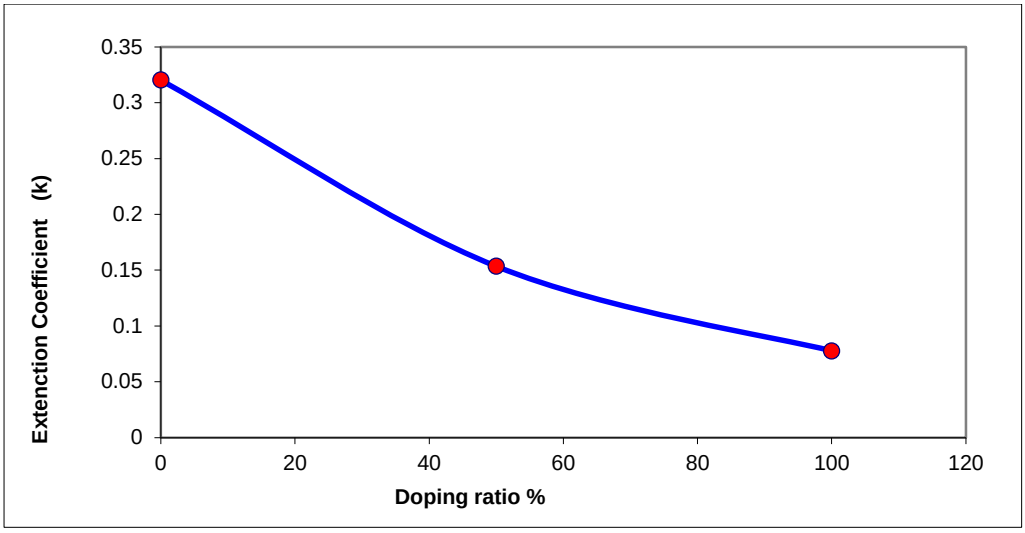

(a)

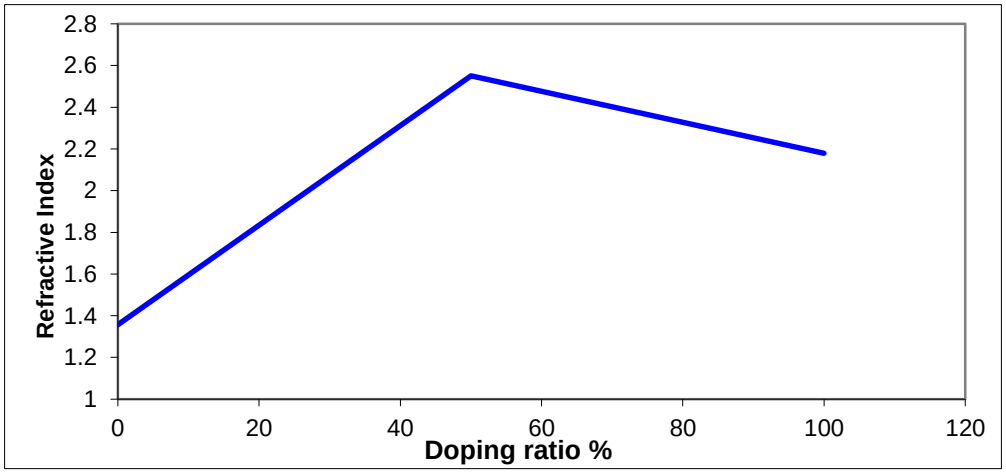

(b)

Figure (3.14): (a) The refractive index has a maximum value for the reflectivity, (b) Represents the refractive index.

Table (3.19) Represents the value of extenction coefficient (K) and refractive index (n).

Doping ratio %	*Extenction coefficient (K)*	*Refractive index (n)*
0 (G)	0.320	1.357
50 (G-Al)	0.153	2.550
100 (Al)	0.077	2.179

4) Energy gap (E_g) and Optical Conductivity (σ):

Energy gap increases non-linearly until it reaches the saturation point, after which the increase of Al has no effect on the energy gap. Because of the vaccination rate is 50%, the practical results were acceptable, but the effect is clear in the region of (0 – 50) % of the doping.

Practically, the energy gap was calculated from the following equation

(Eg = $\frac{1240}{\lambda_{max}}$), whereas, the energy gap of pure graphene is approximately equal (1.7eV) for theoretical and practical measurements.

With doping, the calculation of energy gap is theoretically and practically different due to the different percentage of adding Al atoms. After doping, the energy gap has changed due to the generation of secondary levels, as well as impurities and crystal defects that cause a change in the energy gap. Figure (3.15) shows the energy gap of the samples under study.

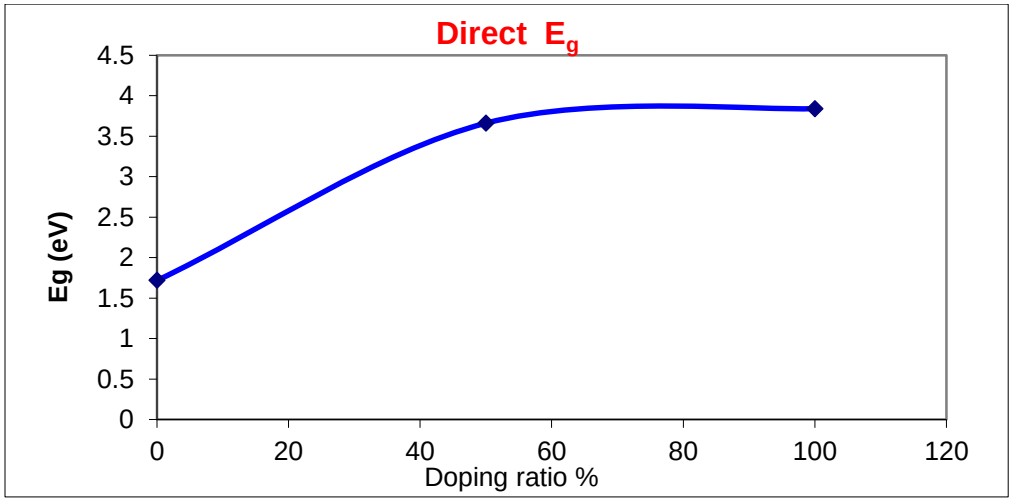

Figure (3.15): Shows the energy gap of the samples under study.

While $\sigma_{Optical}$ decreases with the increase in the proportion of Al, as in Figure (3.16).

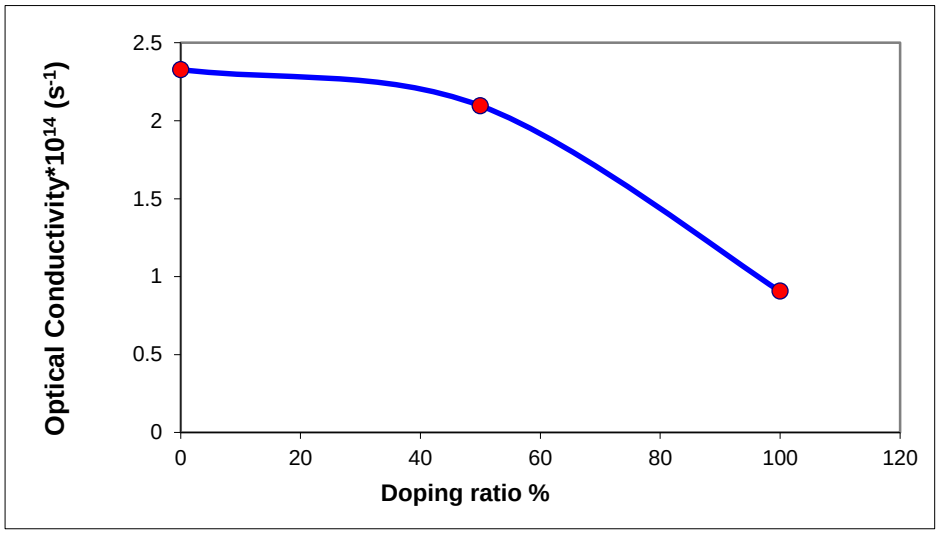

Figure (3.16): Represents Optical Conductivity.

Chapter Four
Conclusions and Future Works

4-1 Conclusions

The main conclusions, that deduced from our results for pure and doped graphene nano-ribbon used DFT method at basis set 6-31G and hybrid function B3LYP, are as follows:

1- Geometrical properties include bonds length and bonds angles for pure and doped nano-ribbon have good agreements with the experimental results.
2- The doped graphene nano-ribbon by aluminium and sulfur atom modification geometrical, electronic and optical properties can be utilized as detector devices
3- Geometrical, electronic, optical proprieties for systems under study has high chemical adsorption compared with physical adsorption.
4- All systems have chemical adsorption, except NH_3 in pure systems.
5- UV–Visible spectrum calculation show that the spectrum effect only in chemical interaction between gases molecule and surface of nano systems.
6- Absorbance decreases with the increase in the proportion of aluminum. Al has the highest transmittance, opposite the graphene which has the lowest.
7- Calculating the energy gap between the theoretical and experimental parts in our study has approximately equal values.
8- Br_2 gas molecule has high reactivity for all studied systems (pure and doped nano-ribbon) as compared with other gases, due to its chemical activity in nature. Where the study of sensitivity for Br_2 gas molecules considered as a novel study.

4-2 Suggestion for Future Works

1. Study of the possibility of employing graphene nanotube as a sensor for (CO, NH_3 and Br_2) toxic gases by DFT.
2. Investigation ability of zinc-oxide nanotubes to sense some toxic gases using first principle study**.**
3. Study the adsorption energy for toxic gases in pure and sulfur-aluminium doped carbon nanotube.
4. Study of interaction energy for inhibition gases using DFT calculation.
5. Design theoretical nano detector for high toxic gases, arsenic and ghardal using first principle study.

1. A. H. Castro, F. Guinea, R. Peres, K. S. Novoselov, A. S., and A. K.Geim. "***The electronic properties of graphene***". Reviews of Modern Physics, vol.81, no.1, p.109, 2009.
2. J. S. Bunch, S. S. Verbridge, J. S. Alden, A. M. Van Der Zande, J. M. Parpia, H. G. Craighead, and P. L. McEuen. "***Impermeable atomic membranes from graphene sheets***". Nano Letters, vol. 8, no. 8, pp. 2458–2462, 2008.
3. R. Saito, G. Dresselhaus, and M. S. Dresselhaus. "***Physical properties of carbon nanotubes***", vol. 35. World Scientific, 1998.
4. A. D. Zdetsis and E. N. Economou "***A pedestrian approach to the aromaticity of graphene and nanographene: Significance of Huckel's (4n+2) π electron rule***". Journal of Physical Chemistry - Series C, vol. 119, no. 29, pp. 16991–17003, 2015.
5. Y. Zhang, T.-T. Tang, C. Girit, Z. Hao, M. C. Martin, A. Zettl, M. F. Crommie, Y. R. Shen, and F. Wang. "***Direct observation of a widely tunable bandgap in bilayer graphene***". Nature, vol. 459, no. 7248, pp. 820–823, 2009.
6. E. V. Castro, K. S. Novoselov, S. V. Morozov, N. M. R. Peres, J. M. B. L.Dos Santos, J. Nilsson, F. Guinea, A. K. Geim, and A. H. C. Neto. "***Biased bilayer graphene: semiconductor with a gap tunable by the electric field effect***". Physical Review Letters, vol. 99, no. 21, p. 216802, 2007.
7. Z. H. Ni, T. Yu, Y. H. Lu, Y. Y. Wang, Y. P. Feng, and Z. X. Shen. "***Uniaxial strain on graphene: Raman spectroscopy study and band-gap opening***". ACS Nano, vol. 2, no. 11, pp. 2301–2305, 2008.
8. V. M. Pereira, A. H. C. Neto, and N. M. R. Peres. "***Tight-binding approach to uniaxial strain in graphene***". Physical Review B, vol. 80, no. 4, p. 045401, 2009.

9. M. Y. Han, B. Ozyilmaz, Y. Zhang, and P. Kim. "***Energy band-gap engineering of graphene nanoribbons***". Physical Review Letters, vol. 98, no. 20, p.206805,2007.

10. E. l. Blog del, and E. Rubio, ***"Study of the electronic structure of graphene and hydrated graphene***" Special-Issue, Physics World, vol. 13, no. 29, 2013.

11. D. Kasuya, M. Yudasaka, K. Takahashi, F. Kokai, and S. Iijima, "***Selective Production of Single-Wall Carbon Nanohorn Aggregates and Their Formation Mechanism***". J. Phys. Chem. B., vol. 106, no. 19, pp. 4947–4951, 2002.

12. T. J. Bernatowicz, R. Cowsik, P. C. Gibbons, K. Lodders, B. Fegley, S. Amari, and R. S. Lewis, "***Constraints on stellar grain formation from presolar graphite in the Murchison meteorite***". Astrophysical Journal. Vol. 472, no.2, pp. 760–782, 1996.

13. J. M. Carlsson, "***Graphene: Buckle or break***". Nature Materials. Vol. 6, no. 11, pp. 801–2, 2007.

14. A. Fasolino, J. H. Los, and M. I. Katsnelson, "***Intrinsic ripples in graphene***". Nature Materials. Vol. 6, no. 11, pp. 858–61, 2007.

15. O. A. Shenderova, V. V. Zhirnov, and D. W. Brenner "***Carbon nanostructures***". Critical Reviews in Solid State and Materials Sciences, vol. 27, no. 3-4, pp. 227-356, 2006.

16. M. C. Lemme, S. Vaziri, A. D. Smith, and M. Östling. "***Alternative graphene devices: beyond field effect transistors***". In 2012 70th Annual Device Research Conference (DRC), pp. 24a–24b. IEEE, 2012.

17. M. C. Lemme, S. Vaziri, A. D. Smith, J. Li, S. Rodriguez, A. Rusu, and M. Östling. "***Graphene for More Moore and More Than Moore applications***". In 2012 IEEE Silicon Nanoelectronics Workshop (SNW), pp. 1–3. IEEE, 2012.

18. J. J. Yoo, K. Balakrishnan, J. Huang, V. Meunier, B. G. Sumpter, A. Srivas- tava, M. Conway, A. L. Mohana Reddy, J. Yu, R. Vajtai, and P. M. Ajayan. "***Ultrathin planar graphene supercapacitors***". Nano Letters, vol. 11, no.4, pp. 1423–1427, 2011.

19. X. Miao, S. Tongay, M. K. Petterson, K. Berke, A. G. Rinzler, B. R. Appleton, and A. F. Hebard. "***High efficiency graphene solar cells by chemical doping***". Nano Letters, vol. 12, no. 6, pp. 2745–2750, 2012.

20. X. Wang, L. Zhi, and K. Müllen. "***Transparent, conductive graphene elec- trodes for dye-sensitized solar cells***". Nano Letters, vol. 8, no. 1, pp. 323–327, 2008.

21. L. Grande, V. T. Chundi, D. Wei, C. Bower, P. Andrew, and T. Ryhänen. "***Graphene for energy harvesting/storage devices and printed electronics***". Particuology, vol. 10, no. 1, pp. 1–8, 2012.

22. S. Joshi, V.D. Bhatt, H. Wu, M. Becherer, P. Lugli, "***Flexible lactate and glucose sensors using electrolyte-gated carbon nanotube field effect transistor for non-invasive real-time monitorin***". IEEE Sens. J. vol. 17, pp. 4315–4321, 2017.

23. S.M. Salimi, F. Saberkari, A. Rahbarpour, "***Comparison of information content of temporal response of chemoresistive gas sensor under three different temperature modulation regimes for gas detection of different feature reduction methods***". In Journal of Physics: Conference Series vol. 939, no. 1, p. 012005, 2017.

24. P.T. Moseley, "***Solid state gas sensors***". Meas. Sci. Technol., vol. 8, no. 3, pp. 223–237, 1997.

25. C. Simonetta, A. Forleo, L. Francioso, R. Rella, P. Siciliano, J. Spadavecchia, D.S. Presicce, A.M. Taurino, and D.A. Forleo, "***Solid state gas sensors: State of***

the art and future activities". J. Optoelectron. Adv. Mater. Vol. 5, no. 5, pp. 1335–1348, 2003.

26. J. Kong, N.R. Franklin, C. Zhou, M.G. Chapline, S. Peng, K. Cho, and H. Dai, "**Nanotube molecular wires as chemical sensors**". Science, vol. 287, no. 5453, pp. 622–625, 2000.

27. G. J. Cadena, J. Riu, F.X. Rius, "***Gas sensors based on nanostructured materials***". Analyst. vol. 132, no. 11, pp. 1083–1099, 2007.

28. F. Schedin, A.K. Geim, S.V. Morozov, E.W. Hill, P. Blake, M. I. Katsnelson, "***Dtection of individual gas molecules adsorbed on graphene***". Nat. Mater. vol. 6, no. 9, pp. 652–655, 2007.

29. J.T. Robinson, F.K. Perkins, E.S. Snow, Z. Wei, P.E. Sheehan, "***Reduced Graphene Oxide Molecular Sensors***". Nano Lett, vol. 8, no. 10, pp. 3137–3140, 2008.

30. Y. Lu, B.R. Goldsmith, N.J. Kybert, A.T.C. Johnson, "***DNA Decorated Graphene Chemical Sensors***", Appl Phys. Lett, vol. 97, no. 8, p. 083107, 2010.

31. P. E. Turner and S. Duffy, "***Evolutionary ecology of multiple phage adsorption and infection****"*, Bacteriophage ecology: population growth, evolution, and impact of bacterial viruses. Cambridge University Press, Cambridge, 2008.

32. D. M. Ruthven, "***Fundamentals of adsorption equilibrium and kinetics in microporous solids***", in Adsorption and Diffusion, Springer, Berlin, Heidelberg, pp. 1- 43, 2006.

33. J. Rouquerol, F. Rouquerol, P. Llewellyn, G. Maurin, and K. S. Sing, "***Adsorption by powders and porous solids: principles, methodology and applications***", Academic press, 2013.

34. V. Lavrenko, I. Podchernyaeva, D. Shchur, A. D. Zolotarenko, and A. D. Zolotarenko, "***Features of Physical and Chemical Adsorption During***

Interaction of Polycrystalline and Nanocrystalline Materials with Gases", Powder Metallurgy and Metal Ceramics, vol. 56, no. 9-10, pp. 504-511, 2018.

35. G. Crini and P- .M. Badot, "***Application of chitosan, aminopolysaccharide, for dye removal from aqueous solutions by adsorption processes using batch studies: A review of recent literature***", Progress in polymer science, vol. 33, no. 4, pp. 399-447, 2008.

36. C.M. Hussain, "***Carbon Nanomaterials as Adsorbents for Environmental Analysis***", Nanomaterials for Environmental Protection, pp. 217-236, 2015.

37. D. Golberg, Y. Bando, Y. Huang, T. Terao, M. Mitome, C. Tang, and C. Zni, "***Boron nitride nanotubes and nanosheets***", ACS nano, vol. 4, no. 0, pp. 2979-2993, 2010.

38. J. Li, Y. Lu, Q. Ye, M. Cinke, J. Han, and M. Meyyappan, "***Carbon nanotube sensors for gas and organic vapor detection***", Nano letters, vol. 3, no. 7, pp. 929-933, 2003.

39. S. Peng and K. Cho, "***Ab initio study of doped carbon nanotube sensors***", Nano letters, vol. 3, no. 4, pp. 513-517, 2003.

40. Z. Ao, J. Yang, S. Li, and Q. Jiang, "***Enhancement of CO detection in Al doped graphene***", Chemical Physics Letters, vol. 461, no. 4-6, pp. 276-279, 2008.

41. P. Lazar, F. Karlicky, P. Jurečka, M. s. Kocman, E. Otyepková, K. r. Safářová, and M. Otyepka, "***Adsorption of small organic molecules on graphene***", Journal of the American Chemical Society, vol. 135, no. 16, pp. 6372-6377, 2013.

42. C. Christodoulou, A. Giannakopoulos, G. Ligorio, M. Oehzelt, M. Timpel, J. Niederhausen, L. Pasquali, A. Giglia, K. Parvez, and K. Müllen, "***Tuning the electronic structure of graphene by molecular dopants: Impact of the substrate***", ACS applied materials & interfaces, vol. 7, no. 34, pp. 19134- 19144, 2015.

43. S. Novikov, N. Lebedeva, and A. Satrapinski, "***Ultrasensitive NO_2 gas sensor based on epitaxial graphene***", Journal of Sensors, vol. 2015, 2015.

44. S. Sharma and A. Verma, "***A theoretical study of HS adsorption on graphene doped with B, Al and Ga***", Physica B: Condensed Matter, vol. 427, pp. 12-16, 2013.

45. G. Brumfiel, "***Nanotubes cut to ribbons New techniques open up carbon tubes to create ribbons***". Nature. doi:10.1038/news.2009.367, 2009.

46. "***Writing Graphene Circuitry With Ion Pens'***". ScienceDaily. March 27, 2012. Retrieved 29 August 2012.

47. "***ISO/TS 80004-1:2015 - Nanotechnologies – Vocabulary – Part 1: Core terms***". International Organization for Standardization. 2015. Retrieved 8 January 2018.

48. Bierhals, Jürgen "***Carbon Monoxide***". Ullmann's Encyclopedia of Industrial Chemistry. doi:10.1002/14356007.a05_203. ISBN 3527306730, 2021.

49. "***Standard Atomic Weights: Bromine***". CIAAW. 2011.

50. Imani, Khadije, Gholamhossein Jafari, and Mohammad Reza Abolhasani. "***Electronic structure calculation of adsorbate gas molecules on an armchair graphene nanoribbon***", International Scholarly Research Notices 2012.

51. Lin, Xianqing, Jun Ni, and Chao Fang. "***Adsorption capacity of H_2O, NH_3, CO, and NO_2 on the pristine graphene***", Journal of Applied Physics vol. 113, no. 3, p. 034306, 2013.

52. Huang, Xiaolu, et al. "***The NH_3 sensing properties of gas sensors based on aniline reduced graphene oxide***", Synthetic metals, vol. 185, pp. 25-30, 2013.

53. Ghosh, R., Singh, A., Santra, S., Ray, S. K., Chandra, A., and Guha, P. K, "***Highly sensitive large-area multi-layered graphene-based flexible ammonia sensor***", Sensors and Actuators B: Chemical, vol. 205, pp. 67-73, 2014.

54. Kuru, C., Choi, D., Choi, C., Kim, Y. J., and Jin, S. "***Palladium decorated graphene-nanoribbon network for enhanced gas sensing***", Journal of nanoscience and nanotechnology, vol. 15, no. 3, pp. 2464-2467, 2015.

55. Cuong, Nguyen Tien, and Nguyen Manh Tien. "***First-principles studies of CO_2 and NH_3 gas molecules adsorbed on graphene nanoribbons***", VNU Journal of Science: Mathematics-Physics vol. 32, no.2, 2016.

56. S. Aghaei, M. Monshi, I. Torres, and I. Calizo, "***Adsorption and Dissociation of Toxic Gas Molecules on Graphene-like BC_3: A Search for Highly Sensitive Molecular Sensors and Catalysts***", arXiv preprint arXiv, vol. 1706, p. 00774, 2017.

57. Gao, Z., Yang, W., Ding, X., Lv, G., and Yan, W. "***Support effects in single atom iron catalysts on adsorption characteristics of toxic gases (NO_2, NH_3, SO_3 and H_2S)***", Applied Surface Science, vol. 436, pp. 585-595, 2018.

58. L. Fernanda, V. López, S. M. P. Ortin, R. M. Olvera, and E. AgacinoValdés, "***DFT study of CO adsorption on nitrogen/boron doped-graphene for sensor applications***", Journal of molecular modeling, vol. 25, no. 4, p. 91, 2019.

59. Subhan, F., Khan, I., and Hong, J. "***Two-dimensional graphitic carbon nitride (g-C4N3) for superior selectivity of multiple toxic gases (CO, NO_2, and NH_3)***" Nanotechnology, vol. 31, no. 14, p. 145501, 2020.

60. Cuong, N. T. "Gas Sensors Based on U-shaped Graphene Nanoribbons: A first-principles Study". VNU Journal of Science: Mathematics-Physics, vol. 36, no. 1, 2020.

61. E. Salih, and A. I. Ayesh, "***Enhancing the sensing performance of zigzag graphene nanoribbon to detect NO, NO_2, and NH_3 gases***". Sensors, vol. 20, no.14, p. 3932, 2020.

62. Ahmed I. Abdelamir, Ehssan Al-Bermanya) and Fouad Sh. Hashim. "***Important Factors Affecting the Microstructure and Mechanical Properties of PEG/ GO-***

Based Nanographene Composites Fabricated Applying Assembly-Acoustic Method". AIP Conference Proceedings. vol. 2213, no. 1, p. 020110, 2020.

63. Mi, T. Y., Triet, D. M., and Tien, N. T. "***Adsorption of gas molecules on penta-graphene nanoribbon and its implication for nanoscale gas sensor***", Physics Open, vol. 2, p. 100014, 2020.

64. V. Haridas, A. Sukhananazerin, J. M. Sneha, B. Pullithadathil, and B. Narayanan, "***α-Fe_2O_3 loaded less-defective graphene sheets as chemiresistive gas sensor for selective sensing of NH_3***". Applied Surface Science, vol. 517, p. 146158, 2020.

65. F. Mofidi and A. Reisi-Vanani, "***Investigation of the electronic and structural properties of graphyne oxide toward CO, CO_2 and NH_3 adsorption: A DFT and MD study***", Applied Surface Science, vol. 507, p. 145134, 2020.

66. J. Kim, Y. Yamada, and S. Sato, "***Bromination Reactivity of Oxygen-Terminated Edges of Graphene***", Journal of Nanoscience and Nanotechnology, vol. 21, no. 5, pp. 3004-3009, 2021.

67. E. Salih, and A. I. Ayesh, "***Pt-doped armchair graphene nanoribbon as a promising gas sensor for CO and CO_2: DFT study***". Physica E: Low-dimensional Systems and Nanostructures, vol. 125, p. 114418, 2021.

68. R. Mehla, and S. Singh, "***Phosphorus doped armchair graphene nanoribbon as a sensing platform of NH_3 detection: A DFT investigation***", Materials Today Proceedings, 2021.

69. Y. Han, G. Liu, B. Sun, J. Shi, M. Wu, B. Xu, and C. Ouyang, "**Penta-graphene as a Metal-free catalyst for CO and NO reaction-Insights from First-principles calculations**", Applied Surface Science, vol. 565, p. 150515, 2021.

70. S. J. Kheirabadi, R. Ghayour, M. Sanaee, and B. Jooj, "***Selective gas sensor based on bilayer armchair graphene nanoribbon***", Physica E: Low-dimensional Systems and Nanostructures, vol. 129, p. 114635, 2021.

71. M. A. Al-Seady, E. Ahmed, H. M. Abduljalil, and A. A. R. Kahewish, "Studying the adsorption energy of CO gas molecule in different nano-systems using density function theory", Egyptian Journal of Chemistry, vol. 64, no. 5, pp. 2607-2612, 2021.

72. R. D. Lide, "***Handbook of chemistry and physics***", CRC Press LLC, USA, vol. 85, 2004.

73. Y. Wang, "***Computational chemistry: a practical guide for applying techniques to real world problems***", John Wiley and Sons, 2004.

74. Y. Wang, "***Theoretical Studies on Water Splitting Using Transition Metal Complexes***", KTH Royal Institute of Technology, 2014.

75. E. Kaxiras, "***Atomic and electronic structure of solid***", Cambridge University Press, New York, USA, 2003.

76. E. F. Valeev and C. Sherrill, "***The diagonal Born-Oppenheimer correction beyond the Hartree-Fock approximation***", Journal of Chemical Physics, vol. 118, no. 9, 2003.

77. V. Sahni, "***Quantal DensityFunctional Theory II:Approximation Methods and Applications***", Springer-Verlag, Berlin Heidelberg, 2010.

78. P. Hohenberg and W. Kohn, phys. Rev. vol. 136, no. 3B, p. 864, 1964.

79. V. Sahni, "***Quantal DensityFunctional Theory II:Approximation Methods and Applications***", Springer-Verlag, Berlin Heidelberg, 2010.

80. M. Troyer, "***Computational Physics***", ETH Zürich, p. 238, 2003.

81. D. W. Rogers, "***Computational Chemistry Using the PC***", 3rd ed., John Wiley & Sons, Inc., Hoboken, New Jersey, 2003.

82. E. Jeffrey and R. Reimers, "***Computational Methods for Large systems: Electronic Structure Approaches for Biotechnology and Nanotechnology***", The University of Sydney, Australia, 2006.

83. D. D. FITTS, "***Principles of Quantum Mechanics: as Applied to Chemistry and Chemical Physics***", Cambridge University Press, New York, 2002.

84. D. W. Rogers, "***Computational Chemistry Using the PC***", 3rd ed., John Wiley and Sons, Inc., Hoboken, New Jersey, 2003.

85. M. Mueller, "***Fundamentals of Quantum Chemistry: Molecular Spectroscopy and Modern Electronic Structure Computations***", Kluwer Academic/Plenum Publishers, New York, 2001.

86. V. Sahni, "***Quantal Density Functional Theory II: Approximation Methods and Applications***", Springer-Verlag, Berlin Heidelberg, 2010.

87. M. J. Mohammed, "***The Molecular Geometry and Electronic Structure of Some Macromolecules***", Ph.D. Thesis, University of Basrah, 2005.

88. W. Koch, M. C. Holthausen, "***A Chemist's Guide to Density Functional Theory***", 2nd ed., Wiley-VCH Verlag GmbH, Germany, 2001.

89. G. Robert, D.Yang, Weitao, "***Density-Functional Theory of Atoms and Molecules***", Oxford University Press, 1994.

90. B. K. Lipkowitz, R. Larter, R. T. Cundari, and D. B. Boyd, "***Reviews in computational chemistry***", John Wiley and Sons, Inc., Hoboken, New Jersey, 21, 2005.

91. E. d. Jeffrey and R. Reimers, "***Computational Methods for Large systems: Electronic Structure Approaches for Biotechnology and Nanotechnology***", The University of Sydney, Australia, 2006.

92. C. D. Sherrill, "***Introduction to Electronic Structure Theory***", orgia Institute of Technology, 2002.

93. D. Young, "***Computational Chemistry: A Practical Guide for Applying Techniques to Real-World Problems***", NY: John Wiley and Sons, Inc., New York, 2001.

94. K. Kim, and K. D. Jordan, "***Comparison of Density Functional and MP2 Calculations on the Water Monomer and Dimer***", Journal of Physical Chemistry, vol. 98, pp. 10089-10094, 1994.

95. P.J. Stephens, F. J. Devlin, C. F. Chabalowski, and M. J. Frisch, "***Ab Initio Calculation of Vibrational Absorption and Circular Dichroism Spectra Using Density Functional Force Fields***", Journal of Physical Chemistry, vol. 98, pp. 11623–11627, 1994.

96. H. H. Fadhal. "***Investigate of the Energy Gap, Ionic Charge and Infrared Spectra (IR) Of Ge Nanocrystals***", *Journal of University of Babylon for Pure and Applied Sciences,* vol. 27, no. 3 pp. 151-160, 2019.

97. M.C. Shane, M.Sc. Thesis, University of Western Australia, Department of physics, 2000.

98. R. F. Stewart, "***Small Gaussian Expansions of Slater-Type Orbitals***", The Journal of Chemical Physics, vol. 52, no. 1, pp. 431-438, 1970.

99. G. M. Merdan, "***Self-Consistent Field Calculation for the effect of Pressure and Temperatureonsome Properties of Greyt in Crystal***", M. Sc. Thesis, University of Babylon, 2005.

100. K. A. Saeed, "***A theoretical Study of the Structural Properties and its Correlation with the Bbiological Activity of Stavudine and some Derivatives***", M. Sc. Thesis, University of Kufa, 2010.

101. P.T. Matthews, "***Introduction to Quantum Mechanics***", Mc Graw-Hill, 1974.

102. H. Dorsett, A. White, "***Overview of Molecular Modeling and Ab Initio Molecular Orbital Methods Suitable for Use with EnergeticMaterials***", Deference science and Technology Organization, Australia, 2000.

103. R. R. Gotwals, and C. Shaw, "***A Chemistry Educator's Guideto Molecular Modeling***", 1st Edition, North Carolina School of Science and Mathematics Center, USA, 2008.

104. J. Cramer, "***Essentials of Computational Chemistry: Theories and Models***", John Wiley and Sons Ltd., the Atrium, Southern Gate, Chichester, England, 2nd Edition, 2004.

105. A. Pacheco, "***Electronic Structure Calculations in Quantum Chemistry***", HPC Training Louisiana State University, 2011.

106. F. Jensen, "***Introduction to Computational Chemistry***", John Wiley and Sons Ltd., the Atrium Southern Gate, Chichester, England, 2nd Edition, 2007.

107. R. Gotwals and S. Sendlinger, "***Molecular Modeling***", North Carolina High School Computational Chemistry Server, Durham, NC, 2006.

108. W. Ochterski, "***Geometry Optimizations in Gaussian***", Gaussian, Incorporation, Wallingford CT., 1999.

109. A. Hinchliffe, "***Molecular Modelling for Beginners***", John Wiley and Sons Ltd, Manchester, 2003.

110. Z. Truhlar, "***Design of Density Functionals That are Broadly Accurate for Thermochemistry, Thermochemical Kinetics, and Nonbonded Interactions***", J. Physics Chemistry, vol. 109, pp. 5656-5667, 2005.

111. H. Hassan, "***A Study of the Electronic Structure of Germanabenzene Molecules***", M. Sc. Thesis, University of Babylon, College of Science, Department of Physics, 2011.

112. M. Weinert, E. Wimmer and J. Freeman, "***Materials Design Application Note***", Phys. Rev., vol. 26, pp. 1-6, 2008.

113. H. Hugosson, "***A Theoretical Treatise on the Electronic Structure of Designer Hard Materials***", Literature publishes, Wilhelm, 2001.

114. A. Ali, "***Investigations of Some Antioxidant Materials By Using Density Functional and Semiempirical Theories***", Ph. D. Thesis, University of Basrah, College of Science, Department of Physics, 2009.

115. A. Camargo, K. Honorio, R. Mercadante, F. Molfetta, C. Alves and A. Dasilva, "***A study of Neolignan Compound with Biological Activity Against Paracoccidioides Brasiliensis by Using Quantum Chemical and Chemometric Methods***", J. Braz. Chem. Soc., vol. 14 , pp. 809, 2003.

116. A. Mlayah, R. Carles, A. Sayari, R. Chtourou, F. Charfi, and R. Planel, "***Resonant Raman scattering in GaAs/AlAs superlattices: The role of electron state mixing***", Phys. Rev. vol. 75, p. 245201, 2007.

117. C. Gatzke, S. Webb, K. Fobelets, and R. Stradling, "***In situ Raman spectroscopy of the selective etching of antimonides in GaSb/AISb/InAs heterostructures***", Semiconductor science and technology, vol. 13, no. 4, p. 399, 1998.

118. J. Piprek, "***Semiconductor optoelectronic devices: introduction to physics and simulation***", Elsevier, 2013.

119. M. A. Mohammed and H. M. Abduljalil, "***A Study of some Environmental Application of Graphene and Boron-Nitride Nano-Ribbon using Density Functional Theory (DFT)***", Babylon University, M.Sc. 2020.

120. A. Y. T. Ayat, I. A. Hamid and S. A. Rabab "***Study of the Structural, Electronic and Spectroscopic Properties of Graphene NanoRibbons*** ", Babylon University, M.Sc. 2016.

121. E. Ahmed, and H. M. Abduljalil "***Effect of NH_2 Substituent Group on PC61BM Properties Using DFT***". International Journal of Emerging Trends in Engineering Research, vol. 7,no. 8, pp. 183-190, 2019.

الخلاصة

استخدمنا شرائط الجرافين النانوية النقية والمطعمة لتحديد الغازات السامة وهي البروم (Br_2) والأمونيا (NH_3) وأحادي أكسيد الكربون (CO) تبحث الدراسة الحالية في استخدام شريط الجرافين النانوي في الحالة النقية والمطعمة كمستشعر للغاز واستخدامه في الطاقة المتجددة.

الحسابات الكمية المستخدمة في الدراسة الحالية هي نظرية دالة الكثافة (DFT) ونظرية دالة الكثافة المعتمدة على الزمن (TD-DFT). تستخدم DFT لحساب خصائص الحالة الأرضية مثل الخصائص الهندسية والطاقة الكلية وفجوة الطاقة وطاقة التأين والالفة الإلكترونية وطاقة الامتزاز. تم استخدام طريقة TD-DFT للحالات المتهيجة مثل الطيف المرئي (الاشعة فوق البنفسجية). يُظهر حساب التركيب الهندسي أن كل أطوال الاواصر للشريط النانوي النقي والمطعم يكون مقارب مع النتائج التجريبية. أيضا الشريط النانوي المطعم بذرة الكبريت (S) او بـذرة الألمنيوم (Al) يعمل على تمديد تركيب الجرافين كعلامة على تعديل خصائص الشريط النانوي.

نظريًا، تم اختيار شريط نانوي يتكون من 116 ذرة بأبعاد N = 4 وM = 4 وطول شريط النانو يساوي (1.4 نانومتر). تم إجراء عملية الامتزاز لكل من الغازات السامة التالية (الأمونيا والبروم وأول أكسيد الكربون. تم تطعيم الأشرطة بأربع ذرات كبريت في مواقع محددة لغرض تحسين الحساسية للغازات المذكورة. ثم تم استبدال ذرات الكبريت بذرات الألومنيوم لنفس الغرض.

عمليًا، تم استخدام طريقة الصب لتحضير أغشية رقيقة لكل من أغشية الجرافين G والألومنيوم Al والجرافين-الألمنيوم G-Al بنسب معينة من هذه الخلائط. لوحظ أن الجرافين مستقر لجميع الأطوال الموجية. كما لوحظ أن الامتصاص يتناقص مع زيادة نسبة الألمنيوم. Al لديه أعلى نفاذية ، مقابل الجرافين الذي لديه أدنى نفاذية.

يُظهر حساب طاقة الامتزاز لشريط الجرافين النانوي النقي أن له تفاعلًا عاليًا مع غاز البروم Br_2 مقارنةً بـالغازات الأخرى (NH_3,CO). تظهر أيضًا طاقة الامتزاز أن غاز Br_2 وCO يتفاعلان كيميائيًا مع سطح شريط الجرافين النانوي. غاز الامونيا له تفاعل فيزيائي مع سطح الشريط. يقوم الشريط النانوي من الجرافين المطعم بـ S وAl بتعديل طاقة الامتزاز وهذا واضح في S-doped .تغير تفاعل NH_3 من الامتزاز الفيزيائي إلى الكيميائي. يتميز غازBr_2 في جميع الأنظمة بتفاعلية عالية مع السطح (الجرافين النقي، والمطعم بـ S، والمطعم بـ Al).

تظهر الحسابات الطيف المرئي للأشعة فوق البنفسجية أن جزيء الغاز التفاعلي مع سطح شريط الجرافين النقي له تحول أحمر. الشريط النانوي Al-doped له إزاحة نحو المنطقة الحمراء للإشعاع الكهرومغناطيسي. أخيرًا، الشريط النانوي S-doped يحتوي على إزاحة نحو الاطوال الموجية الزرقاء للإشعاع الكهرومغناطيسي.

فجوة الطاقة في الجزئين النظري والعملي في دراستنا لها قيم متساوية تقريبًا.

وزارة التعليم العالي والبحث العلمي

جامعة بابل
كلية العلوم
قسم الفيزياء

إمكانية توظيف أشرطة الجرافين النانوية كمتحسس لبعض الغازات السامة بأستخدام نظرية دالية الكثافة

رسالة مقدمة إلى قسم الفيزياء – كلية العلوم – جامعة بابل
وهي جزء من متطلبات نيل درجة الماجستير في العلوم / الفيزياء

من قبل الطالبة

نور الهدى صالح هادي جابر

بكالوريوس في الفيزياء ٢٠١٧-٢٠١٨

بأشراف

أ.د. حيدر محمد عبد الجليل الحفاجي

أ.د. رباب سعدون عبدون

١٤٤٣هـ

٢٠٢١م